Visualizing the organization and differentiation of the male-specific nervous system of *C. elegans*

Tessa Tekieli[1], Eviatar Yemini[1], Amin Nejatbakhsh[2], Chen Wang[1], Erdem Varol[2], Robert W. Fernandez[1], Neda Masoudi[1], Liam Paninski[2] and Oliver Hobert[1,*]

[1] Department of Biological Sciences, Howard Hughes Medical Institute, Columbia University, New York, NY, USA

[2] Departments of Statistics and Neuroscience, Grossman Center for the Statistics of Mind, Center for Theoretical Neuroscience, Zuckerman Institute, Columbia University, New York

*correspondence at: or38@columbia.edu

Summary statement: A multicolor transgene, NeuroPAL, is used to differentially label all male-specific neurons of *C. elegans,* thereby providing landmarks for gene expression, neuronal activity and cell fate analysis.

ABSTRACT

Sex differences in the brain are prevalent throughout the animal kingdom and particularly well appreciated in the nematode *C. elegans*, where male animals contain a little studied set of 93 male-specific neurons. To make these neurons amenable for future study, we describe here how a multicolor reporter transgene, NeuroPAL, is capable of visualizing the distinct identities of all male specific neurons. We used NeuroPAL to visualize and characterize a number of features of the male-specific nervous system. We provide several proofs of concept for using NeuroPAL to identify the sites of expression of *gfp*-tagged reporter genes and for cellular fate analysis by analyzing the effect of removal of several developmental patterning genes on neuronal identity acquisition. We use NeuroPAL and its intrinsic cohort of more than 40 distinct differentiation markers to show that, even though male-specific neurons are generated

throughout all four larval stages, they execute their terminal differentiation program in a coordinated manner in the fourth larval stage. This coordinated wave of differentiation, which we call “just-in-time" differentiation, couples neuronal maturation programs with the appearance of sexual organs.

INTRODUCTION

It is generally appreciated that nervous systems are sexually dimorphic on a gross anatomical level. However, sex differences in nervous systems have been carefully mapped out, with single-cell resolution, in only very few animals. The nematode *C. elegans* is the only organism for which a complete cellular, lineage, and anatomical map of the entire nervous system has been described for both sexes (**Fig.1A,B**)(Cook et al., 2019; Jarrell et al., 2012; Sulston et al., 1980; Sulston and Horvitz, 1977). With 383 neurons total, the nervous system of the male is almost 30% larger than that of the hermaphrodite (302 neurons). Based on lineage and anatomy and molecular profiles, 294 neurons are shared between both sexes. Hermaphrodites, which are somatic females, contain an additional 8 hermaphrodite-specific neurons that fall into two classes: the well characterized HSN and VC motor neuron classes, both of which control egg laying behavior (Schafer, 2005). The male contains an additional 93 neurons that fall into 27 anatomically distinct classes (**Fig.1A,B, Table S1**)(Cook et al., 2019; Molina-Garcia et al., 2020; Sammut et al., 2015; Sulston et al., 1980), two located in the head (sensory neuron classes CEM and MCM), two in the the ventral nerve cord (motor neuron classes CA and CP), while the remaining, heavily interconnected 23 classes are located in the tail of the animal. With the exception of the four CEM sensory neurons in the head, which are born in the embryo and induced to die in hermaphrodites, all male-specific neurons are generated during postembryonic development from blast cells that proliferate, survive and differentiate in a male-specific manner (**Fig.1B**)(Sulston et al., 1980). Based on cell divisions patterns, the 89 postembryonically generated male-specific neurons are generated at different larval stages. Each individual larval stage contributes to the generation of some of these postembryonic neurons (Sulston et al., 1980). However, when exactly these neurons

terminally differentiate is poorly understood. Moreover, in his classic lineage studies Sulston also noted that the number of two male-specific neuron classes, DX and EF, display a variable number of class members (Sulston et al., 1980). However, this observation was originally based on Nomarski optics and limited sample size. Similar variabilities in cell cleavage patterns have not been observed elsewhere within or outside the nervous system of *C. elegans*.

Despite many interesting aspects of the male nervous system, it has received little attention over the years when compared to the nervous system of the hermaphrodite. A number of studies have illuminated aspects of the development and function of male-specific neurons, but those studies only dealt with a limited set of neurons (Barr et al., 2018; Emmons, 2014, 2018; Garcia et al., 2001; Garcia and Portman, 2016; Liu and Sternberg, 1995; Portman, 2017). Hence, many aspects of the development and function of the 93 male-specific neurons remain uncharted territory. With some notable exceptions, including the systematic mapping of neurotransmitter identities (Gendrel et al., 2016; Pereira et al., 2015; Serrano-Saiz et al., 2017), marker analysis in the ray sensory neurons (Lints et al., 2004) and ventral nerve cord (Kalis et al., 2014), few molecular markers have been developed that label male-specific neurons. Single-cell transcriptome approaches have so far exclusively focused on the hermaphrodite (Cao et al., 2017; Packer et al., 2019; Taylor et al., 2021). This dearth of molecular markers not only limits the ability to assess, for example, cell fate in specific mutant backgrounds, but also complicates the means by which cellular expression patterns in the male tail can be unambiguously identified.

Here, we address these shortcomings by showing that NeuroPAL, a previously described multicolor transgene that distinguishes all neuron classes in hermaphrodites (Yemini et al., 2021), can also be used to disambiguate the 93 neurons of the male nervous system. We find that the NeuroPAL transgene, which harbors more than 40 promoters that drive the expression of four distinct fluorophores, generates a color map that provides sufficient discriminatory power to reliably identify all male-specific neurons. We provide proof-of-principle examples that show how to use NeuroPAL to identify gene expression patterns in the nervous system, and use the NeuroPAL color map to provide a number of insights into the development of the male-specific nervous system.

RESULTS

NeuroPAL provides discriminatory color barcodes for all male-specific neurons

With the exception of neurotransmitter pathway genes (Gendrel et al., 2016; Lints and Emmons, 1999; Pereira et al., 2015; Serrano-Saiz et al., 2017), few molecular markers have been comprehensively described throughout the entire male-specific nervous system (www.wormbase.org). For several related neuron classes, for example the ray neurons, molecular markers are available, but they do not provide sufficient resolution to distinguish between all individual class members (Lints and Emmons, 1999; Lints et al., 2004). We set out to test whether the NeuroPAL transgene that we previously described for the *C. elegans* hermaphrodite (Yemini et al., 2021) would provide a similarly information rich molecular map of the male-specific nervous system.

The NeuroPAL transgene was designed to provide color codes to all neurons of the *C. elegans* hermaphrodite (Yemini et al., 2021). This was achieved through the judicious use of four fluorophores with separable emission spectra (mTagBFP2, CyOFP1, Tag-RFP-T, mNeptune2.5), expressed under the control of a set of 43 different promoters with overlapping expression profiles (39 neuron-type specific promoters + a synthetic ultra-panneuronal (UPN) driver made up of the *cis*-regulatory elements of 4 distinct, but fused panneuronal promoters) (Yemini et al., 2021). Promoter choices were dictated by the goal of having neighboring neurons display distinct color codes, thereby unambiguously discriminating neighboring neuron identities from one another.

We found that three NeuroPAL transgenes (independently integrated transgenes *otIs696, otIs669* or *otIs670)* distinguish all neighboring male-specific neurons from one another. This is illustrated in the whole-animal overview panel in **Fig.2A** along with large-scale images of all regions of the *C. elegans* nervous system that contain male-specific neurons (**Fig.2B-D, Fig.S1**). The origin of the color code for each neuron is listed in **Table S1**. For several of the neuron classes, we do not know from which driver the fluorophore color derives from, but this is not relevant for providing disambiguation between neighboring neurons. NeuroPAL not only provides color codes for neuron

classes for which few or no molecular markers were previously available, but it also distinguishes neuronal subclasses that could previously not be discriminated. For example, individual subclasses of A- and B-type ray neurons subtypes can all be distinguished based on color code and position (**Fig.2, Table S1**).

Using NeuroPAL to address stereotypy in the male-specific nervous system

We first used NeuroPAL to address questions that relate to stereotypy of the male-specific nervous system. In the original lineage analysis of the male tail, an unusual phenomenon, not observed anywhere else in the entire organism was reported: descendants of the U ectoblast produce variable numbers of DX and EF neurons, a notion indicated by stippled lines in the original lineage diagram (Sulston et al., 1980)(redrawn here in **Fig.1B**). This violates the complete stereotypy and deterministic nature of all other *C. elegans* cell lineages, both neuronal and non-neuronal (Sulston et al., 1980; Sulston and Horvitz, 1977). Moreover, this variability was reported to be restricted to the EF and DX neurons that descend from the U neuroblast and that are located in the preanal ganglion (the EF3 & 4 and DX3 & 4 neurons). In contrast, the DX and EF neurons that are produced from the F neuroblast (EF1 & 2, DX1 & 2), located in the dorsal rectal ganglion, were generated in an apparently invariant manner (Sulston et al., 1980)(**Fig.1B**). However, no quantification of this observation was provided. Because the lineage analysis entirely relied on cleavage pattern alone, it was also not clear to what extent the variably produced DX and EF neurons acquire a differentiated state.

Using the distinctive NeuroPAL color codes for DX and EF neurons, we examined 22 young adult males and found variability in the presence of fully differentiated EF and DX neurons in the preanal ganglion, as assessed by wild-type expression of NeuroPAL colors in these neurons (**Fig.3A**). Within the F-derived dorsorectal ganglion, 22/22 animals invariably showed two fully differentiated DX neurons (DX1 and DX2) and two EF neurons (EF1 and EF2), corroborating the classic lineageing report (Sulston et al., 1980). In the U-derived preanal ganglion, 19/22

animals show one DX and one EF neuron (= DX3 and EF3), 1/22 had one additional EF (= EF4), and 2/22 had one additional EF (= EF4) and one additional DX (= DX4).

The EF and DX neurons are also the neurons with the greatest inter-animal variability in their relative positioning, as inferred by closely considering the overall variability of positioning of both sex-shared, as well as sex-specific neurons in the tail of the animal. We had previously measured positional variability for the neurons in the hermaphrodite head, where the vast majority of neurons are generated embryonically (Yemini et al., 2021) and we observe a similar extent of variability in the male head, despite the addition of six male-specific neurons (**Fig.3B,C; Fig.S2A-C**; **Table S2**). However, in the tail, where the vast majority of the postembryonically added male-specific neurons are located, there is substantially more positional variability, both in the sex-shared neurons as well as in the sex-specific neurons (**Fig.3D-H; Table S2**). The EF and DX neurons stand out in the extent of variability in their positioning. It will be interesting to investigate whether the inter-animal variability in neuronal soma position in the male tail also translates into variability in neuronal process adjacency, and hence connectivity, between individual animals.

Using NeuroPAL to characterize reporter gene expression patterns in the male tail

Compared to the hermaphrodite nervous system, there has been a remarkable scarcity of molecular markers for neurons in the male tail. The vast majority of reporter transgenes that researchers generate to analyze the expression of their gene of interest are usually only examined in hermaphrodites. One reason for the reluctance of identifying sites of reporter gene expression in the male tail has been the absence of reliable landmark reporters for most male-specific neurons. The fluorescence emission properties of NeuroPAL are designed to be separable from those of GFP signals. This allows researchers to overlay a GFP signal from a reporter gene of interest onto the neuron-specific color barcodes of NeuroPAL, thus identifying the sites of expression of GFP (or CFP/YFP)-based reporter transgenes. As a proof of principle, we analyzed CRISPR/Cas9-engineered *gfp*-based reporter alleles of three neuropeptide encoding

genes that were previously uncharacterized in males (*flp-3, flp-27* and *nlp-51)*. To do so, we crossed these *gfp*-tagged alleles into a NeuroPAL background. We found that *flp-3::T2A::3xNLS::gfp* was expressed in the male-specific CA1, CA2, CA3, and CA4 neurons, located in the ventral nerve cord, as well as the male-specific R4A and SPV neurons in the tail (**Fig.4A)**. We found that *flp-27::T2A::3xNLS::gfp* was expressed in the male-specific neurons CEMV, CEMD, CA8, CA9, PGA, R7A, and was dimly and variably expressed in R6B as well as the sex-shared neuron ASG **(Fig.4B**) and that *nlp-51::SL2::GFP::H2B* was expressed in the male-specific PVX, R3B, and PHD neurons in the tail and variably in R4B (**Fig.4C)**. In addition, non-dimorphic expression was observed in the sex-shared neurons AIM, RIP, and PVN (**Fig.4C)**. These expression patterns corroborate the molecular diversity of members of the CA-type ventral nerve cord motor neurons, and that of the ray sensory neurons, as noted previously with other markers (Kalis et al., 2014; Lints et al., 2004).

Using NeuroPAL to measure neuronal cell-fate specification in the male tail

As described above, NeuroPAL is an indicator of expression for 39 neuron-type specific genes, as well as 4 panneuronal genes (that are fused together in the “UPN” construct), marking all male-specific neurons. These reporter genes measure a wide variety of phenotypic features of a neuron, including neurotransmitter synthesis and transport, neurotransmitter receptors, neuropeptides, sensory receptors from various families, and even panneuronal features (**Table S1**)(Yemini et al., 2021). The markers therefore provide a panoramic view of the differentiated state of all individual neurons, and this state can be probed for proper execution in mutant backgrounds.

We illustrate the NeuroPAL’s utility for such mutant analysis using three prominent patterning genes: a miRNA (*lin-4*)(Lee et al., 1993), a HOX cluster gene (*egl-5/AbdB*)(Chow and Emmons, 1994), and a proneural bHLH gene *(lin-32/Atonal*)(Zhao and Emmons, 1995). The functions of these genes have been reported for only select parts of the male-specific nervous system (Chalfie et al., 1981; Chow and Emmons, 1994; Zhao and Emmons, 1995). We sought to assess whether their reported defects can be recapitulated and better characterized with NeuroPAL. Furthermore, we

anticipated identifying novel defects in these mutants in previously unexamined parts of the male-specific nervous system. Both of these expectations were fulfilled in all three cases examined, as described in the ensuing sections.

NeuroPAL confirms predicted neuron losses and duplications in *lin-4/miRNA* mutants and identifies additional neuronal defects

Animals lacking the *lin-4* miRNA display an iteration of cellular fates normally executed in the first larval stage (Chalfie et al., 1981; Lee et al., 1993), as inferred mainly from the analysis of the ectodermal V and T ectoblasts in the male. Specifically, based cellular cleavage patterns and neuron-like nuclear morphologies, L1-stage specific T-cell neurons appear to be duplicated, while T-derived ray neurons that are normally generated in late larval stages do not appear to be generated (Chalfie et al., 1981)(redrawn in **Fig.5B**). We extended these previous findings through our ability to visualize neuronal differentiation programs with greater detail using NeuroPAL. We confirmed that T-derived ray neurons are not generated in *lin-4* mutant animals while neurons displaying the color code of the T-cell derived PHC, PHD, PLN, and PVW appear to be duplicated (**Fig.5C**). Similarly, V5-lineage derived ray neurons R1A/B and R2A/B, normally generated in the L4 stage, fail to be generated in *lin-4* mutants (**Fig.5D**).

Cleavage defects in other lineages that produce male-specific neurons (B, Y, U, F) had been noted in *lin-4* mutant males (Chalfie et al., 1981), but whether and to what extent neuronal fate specification was disrupted in these lineages remained unclear. We observed no cells with color codes representative of neurons derived from the B, Y and F-blast cells, which are normally born in late larval stages (**Fig.5C&E**). This parallels the effect of *lin-4* on the late born neurons in the T and V lineage and underscores that in *lin-4* mutants, development is arrested in a juvenile state. The color patterns in the preanal ganglion, where U cell descendants are normally located, was too complex to interpret, and therefore we cannot conclude whether there are defects in this lineage as well.

We also found that the fate of all late born, male-specific neurons that are generated by the P neuroblast, are lost in *lin-4* mutant animals. In the tail, male-specific neuronal cell fates derived from the P10 and P11 lineages (HOA, HOB, etc.) appear to be lost. Lastly, in the ventral nerve cord, we observed a loss of color codes of the CA8-9 and CP8-9 neurons (**Fig.5F**). These neurons are normally generated by a cell division event in the L3 stage, and this division is possibly absent in *lin-4* mutants. In contrast, P-cell derived ventral nerve cord motor neurons, that are generated in both sexes in early larval stages, differentiate normally in *lin-4* null mutants (**Fig.5F**).

NeuroPAL identifies homeotic identity transformations in *egl-5* mutants

The B, Y, U and F ectoblasts, which divide exclusively in males, express the HOX cluster protein EGL-5/AbdB (Ferreira et al., 1999). In *egl-5* mutants, these ectoblasts fail to undergo proper divisions and generate no neurons (Chisholm, 1991). This conclusion was based on light-microscopy criteria, i.e. absence of characteristic dense neuronal nuclei. Using the neuronal cell-fate markers present in the NeuroPAL transgene, we further corroborated this notion: none of the colored neurons that descend from B, Y, U and F (**Fig.1B**) can be observed in *egl-5* mutants (**Fig.6**).

Previous work has revealed an anterior-posterior patterning role of the HOX genes *mab-5* and *egl-5* in the ray lineage (Emmons, 2005). Ray neuron 2 is MAB-5-positive and EGL-5-negative, while ray neurons 3 to 6 are EGL-5-positive (Lints et al., 2004). It was suggested that in *egl-5* mutants, rays 3, 4, and 5 homeotically transform to the fate of ray 2 neurons. With the limited markers available at the time, this suggestion remained tentative (Lints et al., 2004). We verified this suggestion by confirming that color code changes in NeuroPAL are consistent with a ray 2 neuron identity transformation (**Fig.6B**)

Using NeuroPAL, we discovered an additional homeotic identity transformation in the posterior-most, male-specific CA motor neurons. The CA8 and CA9 neurons adopt similar color codes to the more anterior CA7 neuron (**Fig.6C**). These transformations are conceptually similar to the homeotic transformations observed in the sex-shared, posterior-most DA and AS neurons in *egl-5* mutants where the most posterior class

member also transforms its identity to that of the more anteriorly located neuron (Kratsios et al., 2017).

NeuroPAL confirms the proneural function of *lin-32/Ato* in ray lineages and reveals additional proneural function in other lineages

The single ortholog of the proneural Atonal gene in *C. elegans, lin-32,* was initially identified and characterized based on its proneural role in the V5 and V6 ectoblast-derived ray neuron (Zhao and Emmons, 1995). Using NeuroPAL, we observed variable loss of neuronal-fate specification in the ray lineage in *lin-32(tm1446)* mutants in the V5- and V6-derived ray neurons, as evidenced by missing color codes in these neurons, including the panneuronal color (**Fig.6E&F**). The most posterior ray neurons, generated by the T-lineage (**Fig.1B**), are unaffected in *lin-32* null mutants, as are all of the other T-derived neurons (**Fig.6E&F**). Y, U and F-derived neurons, as well as P cell-derived, male-specific VNC motor neurons (see lineage diagram in **Fig.1B**) are also unaffected in *lin-32* mutants (**Fig.6G&H**). However, within the B lineage, we discovered a novel proneural role of *lin-32* mutants. While the neurons generated by the posterior daughter of the B ectoblast cell (DVE and DVF, located in the dorsorectal ganglion) differentiate normally, the neuronal cell fates generated by the anterior daughter of B (mostly spicule neurons) cannot be detected (**Fig.6E&G**).

NeuroPAL reveals a coordinated differentiation wave that is concomitant with male tail retraction

We next used NeuroPAL as a tool to provide a panoramic view of timing of neuronal differentiation in the male tail. As illustrated in **Fig.1B**, male-specific neurons are generated at multiple distinct developmental stages. Some male-specific neurons are generated in the embryo (CEM neurons), more are generated at the first larval stage (e.g. PVX of the P cell lineage), and they continue to be generated during the L2 stage (e.g. PCB), L3 stage (B and P cell descendants), and L4 stage (mostly ray sensory neurons)(Sulston et al., 1980). Strikingly, we find that despite their distinct

generation time, the expression of the more than 39 terminal differentiation markers (located on the NeuroPAL transgene) are tightly coordinated over a relatively small window during the mid-to-late L4 stage (**Fig.7; Suppl. Fig.S3**). At early L4, color codes are not yet established (**Fig.7**), nor are they at earlier larval stages (**Suppl. Fig.S3**). The mid-to-late L4 stage is concomitant with the beginning of male tail retraction, a sexually dimorphic process that results in the generation of male-specific mating organs (Emmons, 2005; Nguyen et al., 1999; Sulston et al., 1980). The extent of this coordination is striking, not only because of the substantial number of cell types over which we observe this coordination, but also because of the breadth of the distinct molecular features that are covered by these molecular markers. Among the components of this marker set are the *cis*-regulatory elements from four distinct panneuronal genes (*unc-11, rgef-1, ehs-1, ric-19*). Like the neuron-class-specific marker genes, all these elements only begin to drive reporter gene expression during the mid-to-late L4 stage, concomitant mail tail retraction.

None of the markers for which we observed a coordinated, delayed onset during the L4 stage in sex-specific neurons display a delay in sex-shared and embryonically born neurons. That is, all NeuroPAL markers turn on after neuron birth and remain stable throughout all larval stages (**Suppl. Fig.S3**). The best illustration of the specificity of the coordinated expression wave in male-specific neurons are sex-shared neurons that are born in both sexes at similar stages of larval development. We consistently find that in all cases, the NeuroPAL color code turns on shortly after the generation of these neurons (*i.e.*, after their terminal cell division)(**Suppl. Fig.S3**). For example, the sex-shared PDB and VD13 neurons, both close lineal relatives to the male-specific PVX neuron, are born at about the same time as the male-specific PVX (**Fig.1B**). While PVX generates its color code only at the L4 stage, PDB and VD13 generate their color code much earlier, in the late L1 stage that occurs soon after their birth (**Suppl. Fig.S3**). Similarly, L2-generated, male-specific PCB neuron class turn on their color code at the mid-to-late L4 stage, while the L2-generated, but sex-shared RMF neuron class and the L2-generated neurons of the postdeirid lineage generate their color code shortly after their birth (**Fig.7**).

In order to not be entirely reliant on the NeuroPAL transgene in assessing the timing of neuronal differentiation, we examined whether the delayed, coordinated onset of molecular differentiation features can be observed with other reporters as well. To this end, we utilized fosmid-based reporters for three genes, the panneuronally expressed *rab-3* gene (*otIs498),* the synaptic organizer *oig-1 (otIs450)* and the vesicular transporter *unc-47 (otIs564),* as well as three reporter alleles in which endogenous genes were tagged with *gfp* through CRISPR/Cas9 genome engineering, namely the neuropeptide encoding genes *flp-27, nlp-51* and the vesicular glutamate transporter *eat-4.* While *rab-3* is expressed in all male-specific neurons, *oig-1, unc-47, flp-27, nlp-51* and *eat-4* are expressed in select subset of male-specific neurons, generated before the L4 stage. We find that all of these genes only turn on expression in the L4 stage (**Fig.8**). The delay in onset of expression compared to generation of the neuron is too long to be explained by fluorescent protein maturation alone.

Lastly, we asked whether the delayed differentiation onset of male-specific neurons depends on the sexual identity of the animal. To this end, we prevented cell death of the CEM neurons in hermaphrodites, using a canonical *ced-3* mutant allele (Ellis and Horvitz, 1986) and assessed the onset of expression of the CEM differentiation marker *pkd-2::gfp* in these animals. If the proper timing of *pkd-2* induction would require the animal to have a male identity (for example, if male-specific cells are required to induce *pkd-2* expression), *pkd-2::gfp* expression should either not be induced or initiated at an improper stage (e.g. right after the birth of the neurons). However, we find that *pkd-2::gfp* expression is still timed to the L4 stage of *ced-3* mutant hermaphrodites (**Fig.S4**). Hence, male-specific cues are not required to properly time CEM differentiation.

We conclude that earlier born male-specific neurons delay their differentiation until the fourth larval stage to then differentiate in a coordinated manner, concomitantly with the differentiation of sexual organs.

DISCUSSION

The nervous system of the *C. elegans* male contains almost 30% more neurons than the hermaphrodite. The male-specific nervous system is structurally complex and controls the many intricate steps of male-mating behavior (Garcia et al., 2001; Liu and Sternberg, 1995)(Barr et al., 2018; Portman, 2017). From a developmental perspective, it is fascinating to ask how complex interconnected circuitry is established during postembryonic development and integrated with an already existing nervous system. To address the many questions relating to the development and function of the male-specific nervous system, it is of interest to be able to characterize the gene expression within it, the functions of these male-specific genes, and also to visualize male neuronal activity patterns. The tool that we present here, NeuroPAL, presents a major stepping stone to achieve these goals. NeuroPAL enables rigorous analysis of gene expression patterns. Moreover, the ability to combine NeuroPAL with GCaMP-based neuronal activity recordings – as recently shown in the hermaphrodite nervous system (Yemini et al., 2021) – will pave the way to reliably decipher neuronal activity patterns in the male nervous system.

Owing to its ability to visualize the expression of more than 40 distinct genes that measure the live differentiated state of neurons throughout the entire nervous system of both sexes, we have been able to use NeuroPAL to gain novel insights into the development of the male-specific nervous system. We corroborated and extended the findings of an unusual non-stereotypic variability in the generation of a specific set of neurons, the EF and DX neurons. We further refined and also revealed the novel patterning roles of three gene regulatory factors: a Hox cluster gene, a miRNA, and a bHLH transcription factor. Perhaps most interestingly, we used NeuroPAL to reveal that despite their diverse birth dates, male-specific neurons coordinate the acquisition of terminal identity features to within a specific window of time, the mid-to-late fourth larval stage. At this time other non-neuronal mating structures – including fans, rays and spicules – are generated (Emmons, 2005; Nguyen et al., 1999; Sulston et al., 1980). We term this coordinated differentiation “just-in-time” differentiation, to illustrate that neurons only acquire their functional properties once all the “effector systems” of the male-specific nervous system (*i.e.*, all the end organs innervated by the male-specific

neurons) come into existence, and thus only once the mating process becomes physically possible due to the generation of such mating organs. It is important to emphasize the two reasons why “just-in-time” differentiation cannot merely be a reflection of a delay in maturation of the fluorophores with which we measure differentiation programs. First, fluorescent signals are visible in sex-shared neurons immediately after their generation at early larval stages, whereas male-specific neurons that are born concurrently show a delay of up to several larval stages (>24 hours later); in contrast, fluorophore maturation times are known to operate on a much faster scale, with most maturing within <1 hour (Balleza et al., 2018; Cranfill et al., 2016). Second, the birth dates of different male-specific neurons are distinct, yet the onset of fluorophore expression is coordinated to occur at the same time.

The “just-in-time” terminology is adapted from “just-in-time” specific transcriptional programs in metabolic pathways (Zaslaver et al., 2004). Genes that code for specific proteins in the metabolic production machinery display temporal dynamics which ensure that, when a metabolic production pipeline is being ramped up under specific conditions, proteins are generated only when needed in the production pipeline. This allows the machinery to reach a production goal with minimal total enzyme production (Zaslaver et al., 2004).

Coordinated, “just-in-time” differentiation programs are apparent throughout all male-specific neurons. For one of them, the CEM neurons, the delayed onset of differentiation had been previously noted before. The CEM neurons are born in the embryo (and die in hermaphrodites) but were reported to initiate expression of several molecular features, including the putative sensory receptor *pkd-2* and its cholinergic-neurotransmitter phenotype, only by the L4 stage (Lawson et al., 2019; Pereira et al., 2015; Wang et al., 2010). CEM neurons only synapse onto sex-shared neurons that were generated and already differentiated in the embryo (Cook et al., 2019), thus the “just-in-time” differentiation of CEMs at the L4 stage cannot simply relate to the appearance of sex-specific effector cells at the L4 stage. The reason that CEM differentiation is delayed until the L4 stage likely lies in their function: CEM neurons sample mating cues (Narayan et al., 2016; Srinivasan et al., 2008) and hence are not required to operate until the male is sexually mature.

"Just-in-time" differentiation is not unique to male-specific neurons. Hermaphrodite-specific neurons, of which there are only two classes, the HSN and VC neuron classes, had already been reported to acquire their fully differentiated state only in the L4 stage. In the HSN neurons, which are embryonically born, this is best evidenced by the acquisition of its serotonergic neurotransmitter identity, which they acquire at the late L4 stage (Desai et al., 1988). In the VC neurons, which are generated by the late first-larval stage, cholinergic marker gene expression only becomes induced in the L4 stage as well (Pereira et al., 2015). The logic of the "just-in-time" differentiation of the HSN and VC neurons is evident: they innervate vulval musculature that only becomes generated and properly placed during late-larval development (Sulston and Horvitz, 1977).

How is this coordinated, just-in-time differentiation wave genetically specified? For the proper timing of differentiation of the male-specific CEM and hermaphrodite-specific HSN neurons, the heterochronic pathway has been implicated (Lawson et al., 2019; Olsson-Carter and Slack, 2010). This pathway is composed of a series of sequentially activated gene-regulatory factors, including transcription factors, regulatory RNAs and translational regulators (Rougvie and Moss, 2013). However, the effects of this pathway on CEM and HSN timing was shown to be only partial (Lawson et al., 2019; Olsson-Carter and Slack, 2010), suggesting the involvement of other regulatory factors. For example, it can be envisioned that target-derived signals from synaptic partners help to coordinate the timing of "just-in-time" differentiation. Perhaps sex-specific neurons are under a "differentiation arrest" that actively inhibits the execution of terminal differentiation. This notion is again inferred from the CEM and HSN neuron cases, whose identity-specifier, the terminal selector UNC-86 (Lloret-Fernandez et al., 2018; Shaham and Bargmann, 2002), is already present in the CEM and HSN neurons since their birth (Finney and Ruvkun, 1990). While UNC-86 is required for the expression of HSN and CEM differentiation markers that become induced in the L4 stage (Lloret-Fernandez et al., 2018; Shaham and Bargmann, 2002), it is apparently unable to induce these features until the time is right. Correctly-timed induction might thus be achieved by an inhibitory mechanism that prevents UNC-86 function or,

alternatively, by the absence of a critical UNC-86 cofactor, whose expression is temporally controlled.

An intrinsic feature of terminal differentiation programs of many, and perhaps all *C. elegans* neurons, may explain why terminal differentiation of sex-specific neurons appears to be an all-or-nothing event. In many, and perhaps all *C. elegans* neurons, gene expression programs within a neuron are highly coordinated via the activity of terminal-selector transcription factors that become active right after the birth of a neuron in order to initiate terminal differentiation (Hobert, 2016). Triggering the entire differentiation program of a neuron prematurely, *i.e.* before needed, and thus not coordinated with the differentiation of other neurons, may send uninformative or even conflicting signals to the sex-shared nervous system. Just-in-time differentiation, coordinated over multiple cell and tissue types, ensures that individual components of a nervous system only go online once every individual component is set in place.

MATERIAL AND METHODS

Strains. The following mutant alleles were used in this study: *lin-4(e912), egl-5(u202), ced-3(n717)* and *lin-32(tm1446).* The following reporter strains were used: NeuroPAL strains *otIs669; him-5* and *otIs670; him-8* (Yemini et al., 2021). The following fosmid-based reporters were used: *otIs450[oig-1(fosmid)::SL2::GFP], otIs564[unc-47(fosmid)::SL2::mCherry::H2B], and otIs498[rab-3(fosmid)::SL2::NLS::YFP::H2B].* The following CRISPR/Cas9-generated reporter strains were generated by Sunybiotech through insertion of a reporter cassette at the 3' end of the respective gene: *flp-3(syb2634[T2A::3xNLS::GFP])*, *flp-27(syb3213[T2A::3xNLS::GFP]), nlp-51(syb3936[SL2::GFP::H2B])* and *eat-4(syb4257[SL2::GFP::H2B])*. The following promoter-based reported was used: *myIs4[Ppkd-2::GFP + Punc-122::GFP] him-5(e1490)V* (Bae et al., 2006).

Analysis of NeuroPAL color codes of *egl-5, lin-32,* and *lin-4* mutants was performed using the *him-5* mutant to generate males since males of these mutant strains are not competent for mating. To rule out the contribution of the *him-5* mutation to color code changes in mutants we compared the NeuroPAL color codes in naturally induced males versus *him-5* males. We examined all neurons, both sex-shared and male-specific, and found no differences in color code between naturally induced males and *him-5* males.

Microscopy. Worms were anaesthetized using 20 mM sodium azide and were mounted on 5% agarose pads. Images were acquired on a Zeiss LSM880 confocal microscope, equipped with 7 laser lines: 405, 458, 488, 514, 561, 594, and 633 nm and processed using ImageJ software. Gamma was adjusted for maximal color distinction for all images. All reporter and mutant strains were imaged at 40X.

Staging of worms. To obtain worms staged throughout larval development, adult hermaphrodites were allowed to lay eggs for one hour. After one hour, the hermaphrodites were removed from the plates. The plates were then stored at 20°C until the time points corresponding to each larval stage when they were imaged. To capture the early, mid (when the tail hypodermal cells retract), and late L4 stages, worms were imaged ~44 hours, ~52, and ~55 hours respectively after egg laying and storage at 20°C. As there is some variability even within carefully staged worms, each L4 stage was confirmed by the male-tail morphology.

Variability in cell position. To generate the statistical atlases of male neuron positions, their variability, and colors, we used our previously published strategy (Yemini et al., 2021). Briefly, we initialized the atlas to be the point cloud of one of the worms, then iteratively aligned each animal's neuron position point cloud to the current atlas, until all animals were aligned. These point clouds, which represent neuron positions and colors, were extracted from images of 12 male heads and 13 male tails that were manually annotated. Males were age-matched to those used in our previously published hermaphrodite atlas (Yemini et al., 2021). For each neuron, the atlas includes a mean position, mean color, and a covariance matrix representing the variability for the

neuron's position and color across the population of worms. We computed the positions of the male and hermaphrodite neurons using the determinant of the neuron's positional covariance matrix as an estimate of their aligned spatial occupancy volume (**Table S2**). We used these volumes to compute differences in neuron position variability between hermaphrodites and males. To account for color variability resulting from any changes in the imaging hardware (*e.g.*, aging equipment such as excitation lasers) we affine transformed the male atlas colors to those of the hermaphrodite using the sex-shared neurons. Color alignment and histogram matching have been previously shown to be a critical step for downstream analysis in such computations as atlas creation and neural segmentation (Nejatbakhsh et al., 2020; Varol et al., 2020).

ACKNOWLEDGEMENTS

We thank Rene Garcia for help in distinguishing DVE and DVF, Maureen Barr for *pkd-2::gfp,* Laura Pereira for help in generating the male NeuroPAL map, and members of the Hobert lab for comments on the manuscript. This work was funded by the NIH (R37NS039996) and the Howard Hughes Medical Institute.

REFERENCES

Bae, Y.K., Qin, H., Knobel, K.M., Hu, J., Rosenbaum, J.L., and Barr, M.M. (2006). General and cell-type specific mechanisms target TRPP2/PKD-2 to cilia. Development *133*, 3859-3870.

Balleza, E., Kim, J.M., and Cluzel, P. (2018). Systematic characterization of maturation time of fluorescent proteins in living cells. Nat Methods *15*, 47-51.

Barr, M.M., Garcia, L.R., and Portman, D.S. (2018). Sexual Dimorphism and Sex Differences in Caenorhabditis elegans Neuronal Development and Behavior. Genetics *208*, 909-935.

Cao, J., Packer, J.S., Ramani, V., Cusanovich, D.A., Huynh, C., Daza, R., Qiu, X., Lee, C., Furlan, S.N., Steemers, F.J.*, et al.* (2017). Comprehensive single-cell transcriptional profiling of a multicellular organism. Science *357*, 661-667.

Chalfie, M., Horvitz, H.R., and Sulston, J.E. (1981). Mutations that lead to reiterations in the cell lineages of C. elegans. Cell *24*, 59-69.

Chisholm, A. (1991). Control of cell fate in the tail region of C. elegans by the gene egl-5. Development *111*, 921-932.

Chow, K.L., and Emmons, S.W. (1994). HOM-C/Hox genes and four interacting loci determine the morphogenetic properties of single cells in the nematode male tail. Development *120*, 2579-2592.

Cook, S.J., Jarrell, T.A., Brittin, C.A., Wang, Y., Bloniarz, A.E., Yakovlev, M.A., Nguyen, K.C.Q., Tang, L.T., Bayer, E.A., Duerr, J.S.*, et al.* (2019). Whole-animal connectomes of both Caenorhabditis elegans sexes. Nature *571*, 63-71.

Cranfill, P.J., Sell, B.R., Baird, M.A., Allen, J.R., Lavagnino, Z., de Gruiter, H.M., Kremers, G.J., Davidson, M.W., Ustione, A., and Piston, D.W. (2016). Quantitative assessment of fluorescent proteins. Nat Methods *13*, 557-562.

Desai, C., Garriga, G., McIntire, S.L., and Horvitz, H.R. (1988). A genetic pathway for the development of the Caenorhabditis elegans HSN motor neurons. Nature *336*, 638-646.

Ellis, H.M., and Horvitz, H.R. (1986). Genetic control of programmed cell death in the nematode C. elegans. Cell *44*, 817-829.

Emmons, S.W. (2005). Male development. WormBook, 1-22.

Emmons, S.W. (2014). The development of sexual dimorphism: studies of the Caenorhabditis elegans male. Wiley interdisciplinary reviews Developmental biology *3*, 239-262.

Emmons, S.W. (2018). Neural Circuits of Sexual Behavior in Caenorhabditis elegans. Annu Rev Neurosci *41*, 349-369.

Ferreira, H.B., Zhang, Y., Zhao, C., and Emmons, S.W. (1999). Patterning of Caenorhabditis elegans posterior structures by the Abdominal-B homolog, egl-5. Dev Biol *207*, 215-228.

Finney, M., and Ruvkun, G. (1990). The unc-86 gene product couples cell lineage and cell identity in C. elegans. Cell *63*, 895-905.

Garcia, L.R., Mehta, P., and Sternberg, P.W. (2001). Regulation of distinct muscle behaviors controls the C. elegans male's copulatory spicules during mating. Cell *107*, 777-788.

Garcia, L.R., and Portman, D.S. (2016). Neural circuits for sexually dimorphic and sexually divergent behaviors in Caenorhabditis elegans. Curr Opin Neurobiol *38*, 46-52.

Gendrel, M., Atlas, E.G., and Hobert, O. (2016). A cellular and regulatory map of the GABAergic nervous system of C. elegans. eLife *5*.

Hobert, O. (2016). Terminal Selectors of Neuronal Identity. Curr Top Dev Biol *116*, 455-475.

Jarrell, T.A., Wang, Y., Bloniarz, A.E., Brittin, C.A., Xu, M., Thomson, J.N., Albertson, D.G., Hall, D.H., and Emmons, S.W. (2012). The connectome of a decision-making neural network. Science *337*, 437-444.

Kalis, A.K., Kissiov, D.U., Kolenbrander, E.S., Palchick, Z., Raghavan, S., Tetreault, B.J., Williams, E., Loer, C.M., and Wolff, J.R. (2014). Patterning of sexually dimorphic neurogenesis in the caenorhabditis elegans ventral cord by Hox and TALE homeodomain transcription factors. Dev Dyn *243*, 159-171.

Kratsios, P., Kerk, S.Y., Catela, C., Liang, J., Vidal, B., Bayer, E.A., Feng, W., De La Cruz, E.D., Croci, L., Consalez, G.G.*, et al.* (2017). An intersectional gene regulatory strategy defines subclass diversity of C. elegans motor neurons. eLife *6*.

Lawson, H., Vuong, E., Miller, R.M., Kiontke, K., Fitch, D.H., and Portman, D.S. (2019). The Makorin lep-2 and the lncRNA lep-5 regulate lin-28 to schedule sexual maturation of the C. elegans nervous system. eLife *8*.

Lee, R.C., Feinbaum, R.L., and Ambros, V. (1993). The C. elegans heterochronic gene lin-4 encodes small RNAs with antisense complementarity to lin-14. Cell *75*, 843-854.

Lints, R., and Emmons, S.W. (1999). Patterning of dopaminergic neurotransmitter identity among Caenorhabditis elegans ray sensory neurons by a TGFbeta family signaling pathway and a Hox gene. Development *126*, 5819-5831.

Lints, R., Jia, L., Kim, K., Li, C., and Emmons, S.W. (2004). Axial patterning of C. elegans male sensilla identities by selector genes. Dev Biol *269*, 137-151.

Liu, K.S., and Sternberg, P.W. (1995). Sensory regulation of male mating behavior in Caenorhabditis elegans. Neuron *14*, 79-89.

Lloret-Fernandez, C., Maicas, M., Mora-Martinez, C., Artacho, A., Jimeno-Martin, A., Chirivella, L., Weinberg, P., and Flames, N. (2018). A transcription factor collective defines the HSN serotonergic neuron regulatory landscape. eLife *7*.

Molina-Garcia, L., Lloret-Fernandez, C., Cook, S.J., Kim, B., Bonnington, R.C., Sammut, M., O'Shea, J.M., Gilbert, S.P., Elliott, D.J., Hall, D.H.*, et al.* (2020). Direct glia-to-neuron transdifferentiation gives rise to a pair of male-specific neurons that ensure nimble male mating. eLife *9*.

Narayan, A., Venkatachalam, V., Durak, O., Reilly, D.K., Bose, N., Schroeder, F.C., Samuel, A.D., Srinivasan, J., and Sternberg, P.W. (2016). Contrasting responses within a single neuron class enable sex-specific attraction in Caenorhabditis elegans. Proc Natl Acad Sci U S A *113*, E1392-1401.

Nejatbakhsh, A., Varol, E., Yemini, E., Hobert, O., and Paninski, L. (2020). Probabilistic Joint Segmentation and Labeling of C. elegans Neurons (Cham: Springer International Publishing).

Nguyen, C.Q., Hall, D.H., Yang, Y., and Fitch, D.H. (1999). Morphogenesis of the Caenorhabditis elegans male tail tip. Dev Biol *207*, 86-106.

Olsson-Carter, K., and Slack, F.J. (2010). A developmental timing switch promotes axon outgrowth independent of known guidance receptors. PLoS Genet *6*.

Packer, J.S., Zhu, Q., Huynh, C., Sivaramakrishnan, P., Preston, E., Dueck, H., Stefanik, D., Tan, K., Trapnell, C., Kim, J.*, et al.* (2019). A lineage-resolved molecular atlas of C. elegans embryogenesis at single-cell resolution. Science *365*.

Pereira, L., Kratsios, P., Serrano-Saiz, E., Sheftel, H., Mayo, A.E., Hall, D.H., White, J.G., LeBoeuf, B., Garcia, L.R., Alon, U.*, et al.* (2015). A cellular and regulatory map of the cholinergic nervous system of C. elegans. eLife *4*.

Portman, D.S. (2017). Sexual modulation of sex-shared neurons and circuits in Caenorhabditis elegans. J Neurosci Res *95*, 527-538.

Rougvie, A.E., and Moss, E.G. (2013). Developmental transitions in C. elegans larval stages. Curr Top Dev Biol *105*, 153-180.

Sammut, M., Cook, S.J., Nguyen, K.C., Felton, T., Hall, D.H., Emmons, S.W., Poole, R.J., and Barrios, A. (2015). Glia-derived neurons are required for sex-specific learning in C. elegans. Nature *526*, 385-390.

Schafer, W.R. (2005). Egg-laying. WormBook, 1-7.

Serrano-Saiz, E., Pereira, L., Gendrel, M., Aghayeva, U., Battacharya, A., Howell, K., Garcia, L.R., and Hobert, O. (2017). A Neurotransmitter Atlas of the Caenorhabditis elegans Male Nervous System Reveals Sexually Dimorphic Neurotransmitter Usage. Genetics *206*, 1251-1269.

Shaham, S., and Bargmann, C.I. (2002). Control of neuronal subtype identity by the C. elegans ARID protein CFI-1. Genes Dev *16*, 972-983.

Srinivasan, J., Kaplan, F., Ajredini, R., Zachariah, C., Alborn, H.T., Teal, P.E., Malik, R.U., Edison, A.S., Sternberg, P.W., and Schroeder, F.C. (2008). A blend of small molecules regulates both mating and development in Caenorhabditis elegans. Nature *454*, 1115-1118.

Sulston, J.E., Albertson, D.G., and Thomson, J.N. (1980). The Caenorhabditis elegans male: postembryonic development of nongonadal structures. Dev Biol *78*, 542-576.

Sulston, J.E., and Horvitz, H.R. (1977). Post-embryonic cell lineages of the nematode, Caenorhabditis elegans. Dev Biol *56*, 110-156.

Taylor, S.R., Santpere, G., Weinreb, A., Barrett, A., Reilly, M., Xu, C., Varol, E., Oikonomou, P., Glenwinkel, L., McWhirter, R.*, et al.* (2021). Molecular topography of an entire nervous system. Cell *in press*.

Varol, E., Nejatbakhsh, A., Sun, R., Mena, G., Yemini, E., Hobert, O., and Paninski, L. (2020). Statistical Atlas of C. elegans Neurons (Cham: Springer International Publishing).

Wang, J., Schwartz, H.T., and Barr, M.M. (2010). Functional specialization of sensory cilia by an RFX transcription factor isoform. Genetics *186*, 1295-1307.

Yemini, E., Lin, A., Nejatbakhsh, A., Varol, E., Sun, R., Mena, G.E., Samuel, A.D.T., Paninski, L., Venkatachalam, V., and Hobert, O. (2021). NeuroPAL: A Multicolor Atlas for Whole-Brain Neuronal Identification in C. elegans. Cell *184*, 272-288 e211.

Zaslaver, A., Mayo, A.E., Rosenberg, R., Bashkin, P., Sberro, H., Tsalyuk, M., Surette, M.G., and Alon, U. (2004). Just-in-time transcription program in metabolic pathways. Nat Genet *36*, 486-491.

Zhao, C., and Emmons, S.W. (1995). A transcription factor controlling development of peripheral sense organs in C. elegans. Nature *373*, 74-78.

FIGURES

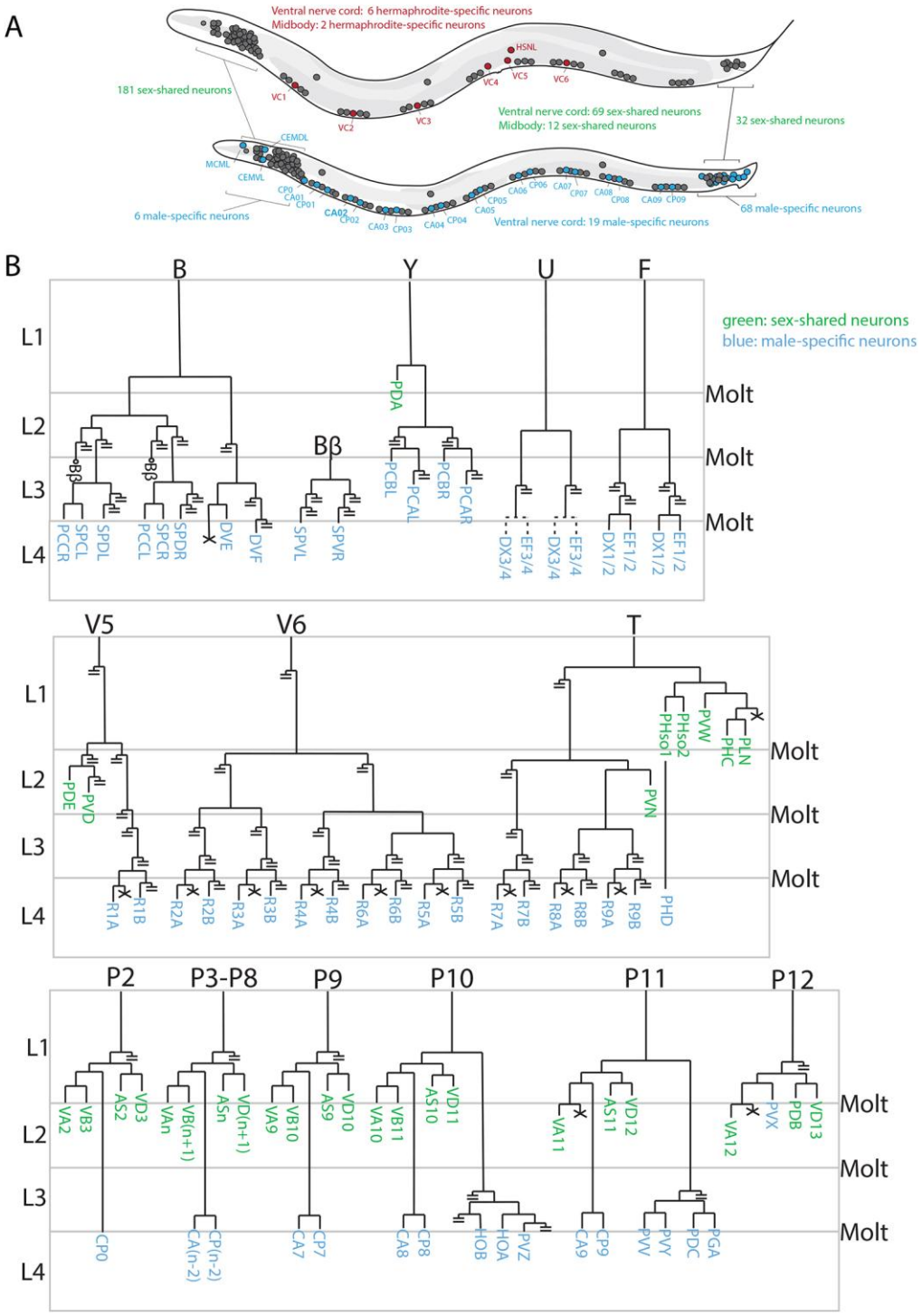

Fig.1: Lineage patterns to illustrate temporal generation

A: Schematic overview of sex-specific nervous systems.

B: Abridged version of the Sulston (1980) lineage diagram of male-specific neurons in the tail. Only those branches that generate neurons are shown till the end, cells that die are denoted with an X, all other branches are cut off (with double strike through). Note that male-specific neurons are generated at different times of larval development, with the earliest being generated in the L1 stage (PVX) and the latest being generated in the early L4 stage (DX, EF, and rays). The lineage of the embryonically generated male-specific CEM neurons is not shown.

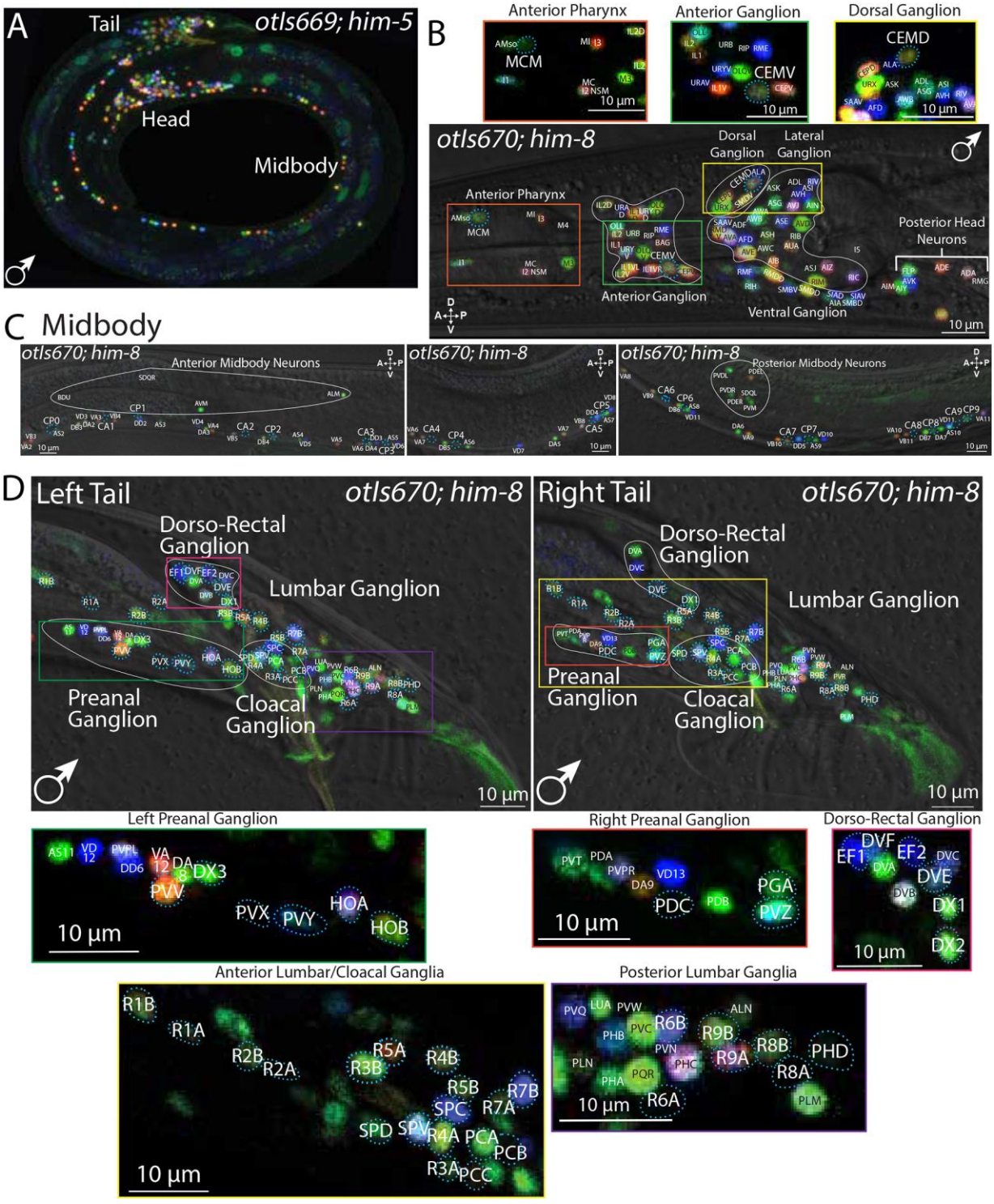

Fig.2: Multicolor map of the adult, male-specific nervous system

A: Overview of entire male NeuroPAL worm (*otIs669;him-5*) with the head, midbody, and tail regions indicated.

B: Micrograph of a stereotypic adult male NeuroPAL (*otIs670; him-8)* head with inset images of regions in the male head containing male-specific neurons. These inset images correspond to the anterior pharynx (outlined in orange), the anterior ganglion (outlined in light green), and the dorsal ganglion (outlined in yellow). All male-specific neurons are indicated with blue dashed circles.

C: Micrographs of stereotypic images from the midbody and ventral nerve cord (VNC) of adult male NeuroPAL (*otIs670; him-8)* worms from anterior to posterior. All male-specific neurons are indicated with blue dashed circles.

D: Stereotypic micrographs of the left and right side of male NeuroPAL tails with zoomed in images of indicated regions below. These zoomed in images correspond to the left preanal ganglion (outlined in green), the right preanal ganglion (outlined in orange), the dorso-rectal ganglion (outlined in magenta), the anterior lumbar/cloacal ganglia (outlined in yellow), and the posterior lumbar ganglia (outlined in purple). All male-specific neuros are indicated with blue dashed circles. In response to our lasers, the male spicules exhibit yellow autofluorescence and the tip of the male fan exhibits green autofluorescence.

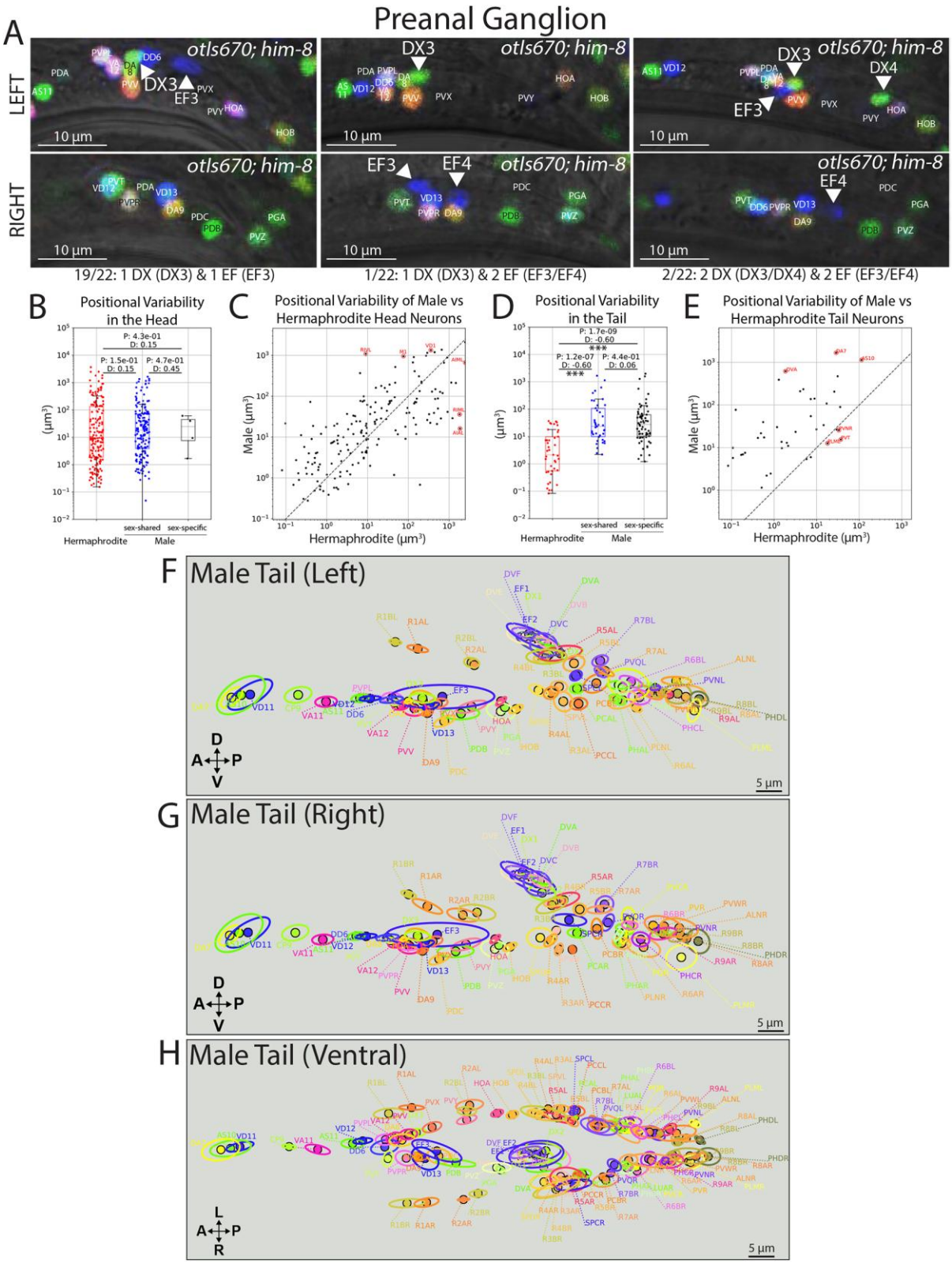

Fig.3: Variability of cell generation and positions in the adult male tail

A: NeuroPAL (*otIs670; him-8*) is used to visualize the variability of DX and EF neuron (DX3 & 4 and EF3 & 4) generation in the preanal ganglion of the adult male tail. Example images of the left and right sides (top and bottom, respectively) of the male preanal ganglion are shown in NeuroPAL worms. These images depict real observations of the indicated number of DX and EF neurons. The fraction of NeuroPAL worms observed, with the indicated DX/EF neuron count, is listed below the set of images exemplifying the indicated numbers of DX and EF neurons. Arrowheads indicate the EF and DX neurons in the images.

B-E: Quantification of positional variability for the collection of all head (B,C) and tail (D,E) neurons of the hermaphrodite (which are all sex-shared) versus the male sex-shared and sex-specific neurons. In the head, the positional variability is nearly the same (B,C). In the tail (D,E), the positional variability for the group of hermaphrodite neurons is far less than that of the male sex-shared and sex-specific neurons. Six neurons that show maximal differences between both sexes are circled and identified (C,E). Shown is the P-value (Mann-Whitney U test) for differences between hermaphrodites and males and the effect size (Cohen's D). For the head N = 10 hermaphrodites, 12 males, 182 sex-shared neurons, and 6 male-specific neurons, with a mean of 9.6 neurons/hermaphrodite and 9.8 neurons/male. For the tail N = 10 hermaphrodites, 13 males, 41 sex-shared neurons, and 69 male-specific neurons, with a mean of 9.6 neurons/hermaphrodite and 11.6 neurons/male.

F-H: The atlas of male tail neuron positional variability (based on 13 male tails) for the left (F), right (G), and ventral (H) sided views. Dots indicate the mean position of each neuron. Ellipses indicate the positional variability of each neuron in the given axis. Neuron colors are caricatured to approximate those in NeuroPAL but have been brightened for visibility.

Further hermaphrodite and male atlases can be found in **Suppl. Fig.S2**. Data is available in **Suppl. Table S2**.

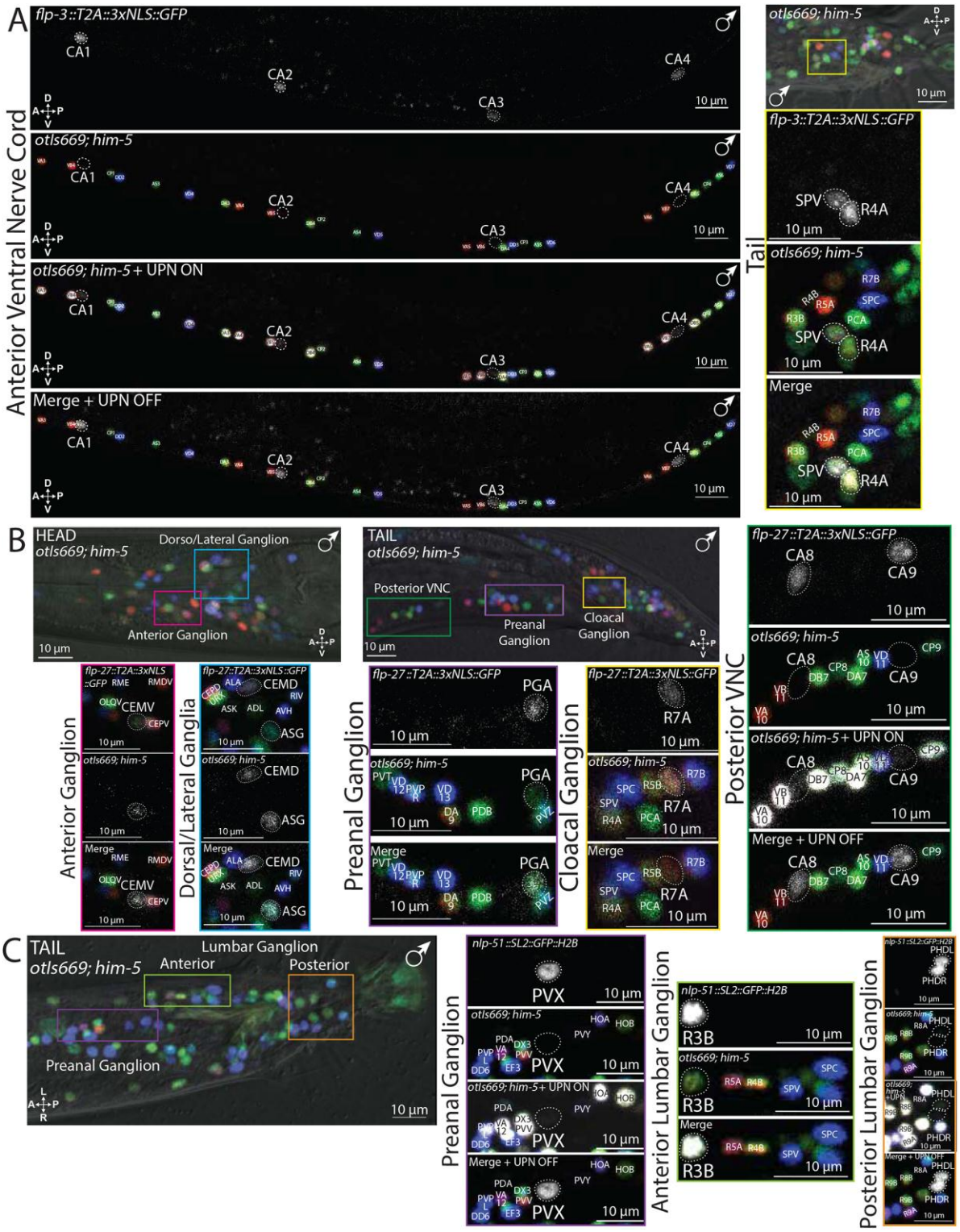

Fig.4: Using NeuroPAL for identification of *gfp*-based expression patterns

A: NeuroPAL (*otIs669; him-5*) is used to identify the GFP expression profile of a *gfp*-tagged neuropeptide gene, *flp-3(syb2634[T2A::3xNLS::GFP])* in the male ventral nerve cord (VNC) and the tail. An overview of the male tail is shown in the top image with inset images (outlined in yellow) below.

B: NeuroPAL is used to identify the GFP expression profile of a *gfp*-tagged neuropeptide gene, *flp-27(syb3213[T2A::3xNLS::GFP])* in the male head, posterior VNC, preanal ganglion and lumbar ganglion. An overview of the head is shown with inset images that correspond to the anterior ganglion (outlined in magenta) and the dorso/lateral ganglia (highlighted in light blue). In the posterior VNC, it is expressed in the male-specific neurons CA8 and CA9, and in the male-specific neuron PGA in the preanal ganglion. In the lumbar ganglion, it is expressed in the male-specific ray neuron R7A, and it is variably dimly expressed (not pictured) in R6B. An overview picture of the male tail is shown with inset images that correspond to the preanal ganglion (outlined in purple), the posterior ventral nerve cord (outlined in green), and the cloacal ganglia (outlined in yellow).

C: NeuroPAL is used to identify the GFP expression profile of a neuropeptide gene, *nlp-51(syb3936[SL2::GFP::H2B)* in the male tail. An overview picture of the male tail is shown with inset images that correspond to the preanal ganglion (outlined in purple), the anterior lumbar ganglion (outlined in light green), and the posterior lumbar ganglion (outlined in light orange). *nlp-51* is also expressed in the sex-shared neurons RIP, AIM, and PVN, as well as variably expressed in the male-specific neuron R4B (not pictured).

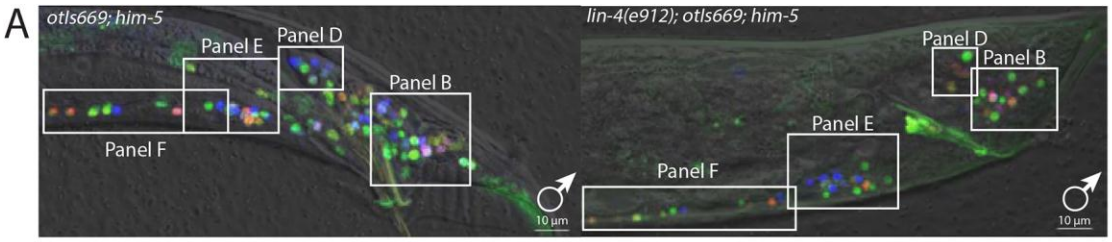

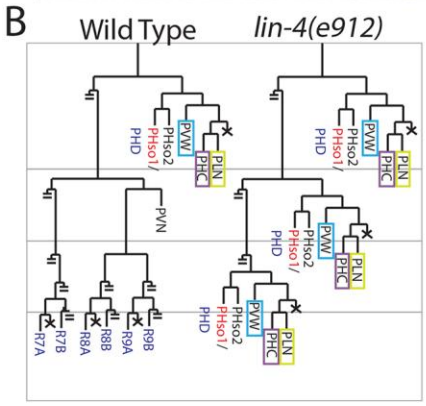

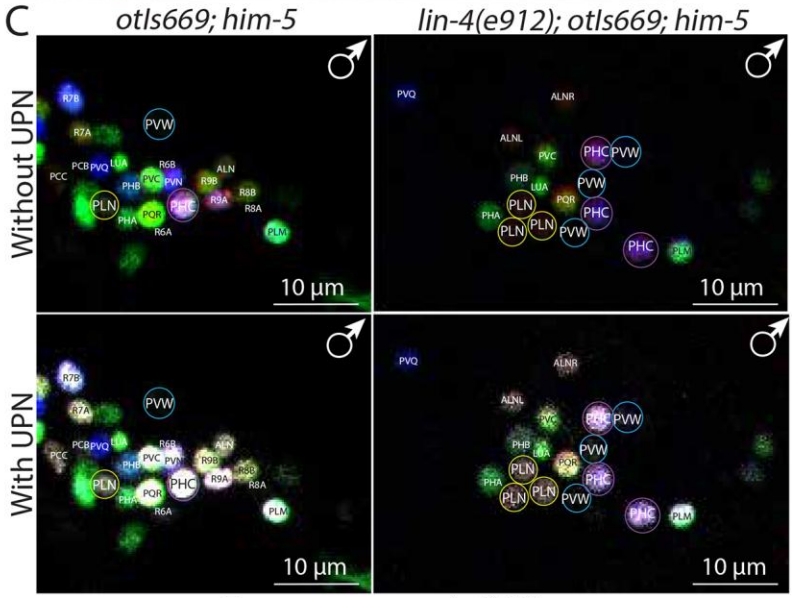

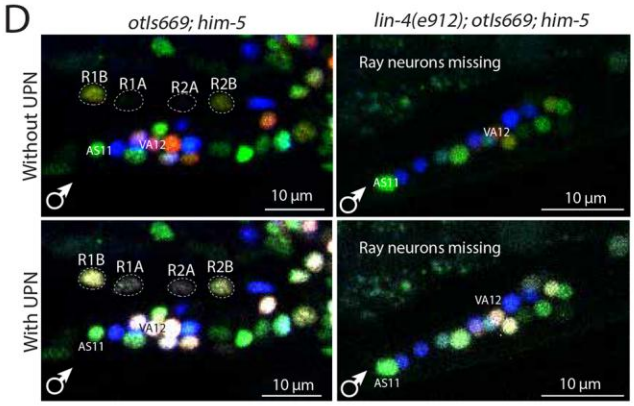

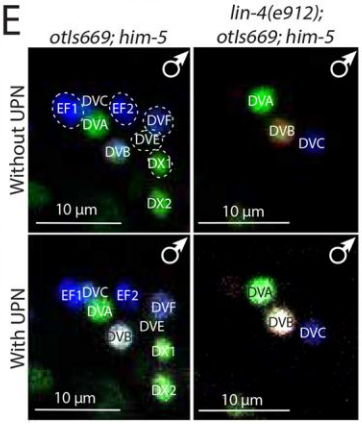

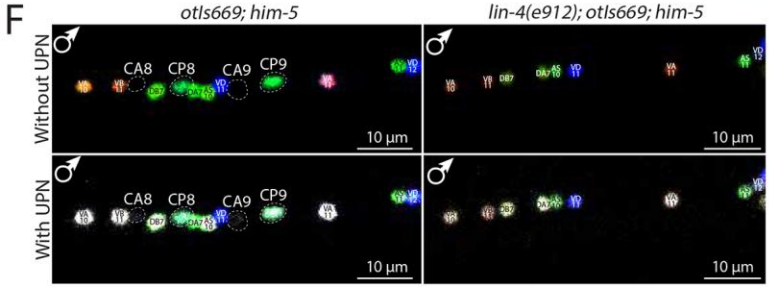

Fig.5: NeuroPAL visualizes neuronal-patterning defects in miRNA *lin-4* mutants

A: Micrographs of the posterior VNC and tails of wild type and *lin-4* mutant males with boxes indicating from which regions each panel was derived.

B: Lineage diagrams depicting the wild-type T lineage on the left and the *lin-4* mutant T lineage exhibiting lineage reiterations in the L1-specific T lineage, as reported by Chalfie *et al.*, 1981. Only those lineage branches containing neurons are depicted to the end, cells that die are represented with an X, and all other branches are cut off (depicted by double strike through). The names of sex-shared neurons are depicted in black, hermaphrodite-specific neurons are depicted in red, and male-specific neurons are depicted in blue.

C: Lineage iterations in the L1-specific T lineage, first reported by Chalfie *et al.*, 1981, are confirmed with NeuroPAL, as evidenced by the presence of additional neurons with the distinct NeuroPAL color barcodes of PLN, PHC, and PVW in the tail of *lin-4(e912)* males. The left image depicts a wild-type male NeuroPAL tail with a single PLN neuron (yellow circle), a single PHC neuron (purple circle), and a single PVW neuron (blue circle). In contrast, the *lin-4(e912)* mutant male tail contains three PLN neurons (yellow circles), three PHC neurons (purple circles), and three PVW neurons (blue circles), all distinguished by their NeuroPAL coloring. 20 animals were scored and all animals exhibited reiterations in the L1-specific T lineage.

D: Male-specific ray neurons (R1A, R1B, R2A, R2B) generated from the V5 lineage, and depicted in dashed circles, are missing in *lin-4(e912)* mutants. Male-specific ray neurons were never observed in the 20 scored worms. Male-specific neurons generated from the B and F lineages in the dorsorectal ganglion (DRG), indicated by dashed circles in the image of NeuroPAL on its own, are missing in *lin-4(e912)* mutants. In contrast, sex-shared neurons (DVA, DVB, and DVC) remain in *lin-4(e912*) mutants. 20 animals were scored and neurons from the B and F lineages in the DRG were never observed.

E: Male-specific neurons generated from the B and F lineages in the dorsorectal ganglion (DRG), indicated by dashed circles in the image of NeuroPAL on its own, are missing in *lin-4(e912)* mutants. In contrast, sex-shared neurons (DVA, DVB, and DVC) remain in *lin-4(e912*) mutants. 20 animals were scored and neurons from the B and F

lineages in the DRG were never observed.

F: The color codes of the L3-specific CA8-9 and CP8-9 neurons in the male VNC are missing in *lin-4(e912)* mutants, while the L1-specific neurons VA, VB, VD are unaffected, as evidenced by the expression of their proper NeuroPAL colors. In the 20 animals that were scored, the color codes of the CA8 and CP8 neurons were never observed, while the color code of CA9 was observed in one animal, and the color code of CP9 was observed in five animals.

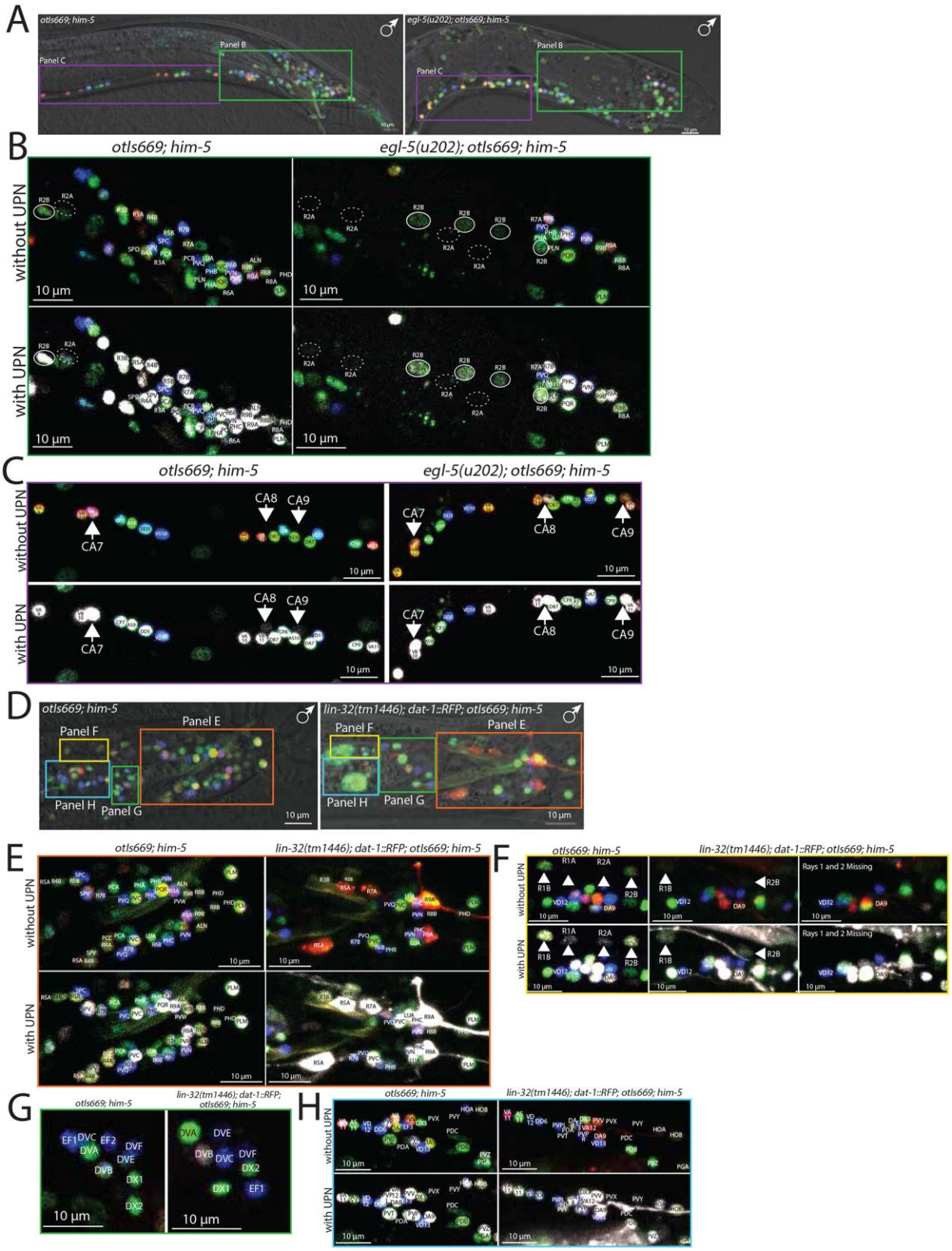

Fig.6: NeuroPAL visualizes patterning defects in transcription factor mutants.

A-C: Patterning defects in the VNC of *egl-5* Hox mutant males are visualized using NeuroPAL (*otIs669; him-8*).

A: Micrographs of the posterior VNC and tails of wild type and *egl-5* mutant males with boxes indicating regions from which each following panel are derived. The region of the tail from which panel B is derived is outlined in green and the region from which panel C is derived is outlined in purple.

B: Transformations of ray neurons, R3, R4, and R5 to that of a R2 neuron fate was described by Lints *et al.*, 2004. Here the A-type neurons (R3A, R4A, R5A) are denoted by dashed circles and the B-type neurons (R3B, R4B, R5B) are denoted by closed circles. In e*gl-5(u202)* mutant males there is a loss of the NeuroPAL colors of the A- and B-type R3, R4, and R5 neurons and a gain of 3 R2A and 3 R2B neurons. The transformation of R3, R4, and R5 was observed in all 14 animals that were scored.

C: The arrows denote CA7, CA8, and CA9 neurons in NeuroPAL and *egl-5(u202)*; NeuroPAL males. CA8 and CA9, normally marked only by the panneuronal marker in NeuroPAL, take on a distinct color, similar to CA7, in *egl-5(u202)* males. CA7, CA8, and CA9 are indicated with arrows in all images. The transformation of CA8 and CA9 neurons was found in all 14 animals that were scored.

D-H: Patterning defects in *lin-32(tm1446)* bHLH mutant animals, visualized with *otIs669.* The *lin-32* mutant strain also carries a cytoplasmic *dat-1::RFP* reporter in the background which marks dopamine neurons and corroborates the defects observed with NeuroPAL. The cytoplasmic *dat-1::RFP* reporter expression is easily distinguished from the nuclear expression of NeuroPAL.

D: Micrographs of the posterior VNC and tails of wild type and *lin-32* mutant males with boxes indicating regions from which each following panel are derived. The region of the tail from which panel E is derived is outlined in orange, panel F is outlined in yellow, panel G is outlined in green, and panel H is outlined in light blue.

E: A representative image of a *lin-32(tm1446)* male depicts variable loss of male ray neurons in the tail. While posterior ray neurons are observed in most *lin-32* mutant male tails, other ray neurons are variably identifiable by their NeuroPAL color. Out of the 15 *lin-32(tm1446)* males that were scored, all showed some defects in ray neurons. Within

the same animal the presence of ray neurons often differed between the left and right side, as pictured.

F: Variable loss of ray neurons R1B and R2B was observed in *lin-32(tm1446)* males. Two example images from *lin-32* mutant males are shown next to a wild-type NeuroPAL image of the region of interest. In the middle *lin-32(tm1446)* image, R1B and R2B are present and properly colored, while in the bottom *lin-32(tm1446)* image both R1B and R2B are missing, thus demonstrating their variability in *lin-32* mutant males. Out of the 15 animals scored, nine had neither R1B nor R2B, three had one R2B, and three had both R1B and R2B.

G: All neurons in the dorsorectal ganglion (DRG) are unaffected in *lin-32(tm1446)* males as evidenced by the preservation of all NeuroPAL colors. Out of the 15 animals scored none of the *lin-32* mutant males showed defects in the DRG.

H: All neurons in the preanal ganglion (PAG) are unaffected in *lin-32(tm1446)* males as evidenced by the preservation of all NeuroPAL colors. Out of the 15 animals scored none of the *lin-32* mutant males showed defects in the PAG.

In panels B-H, the upper images are NeuroPAL without the panneuronal marker (“UPN”-based), while the lower images include this marker in white.

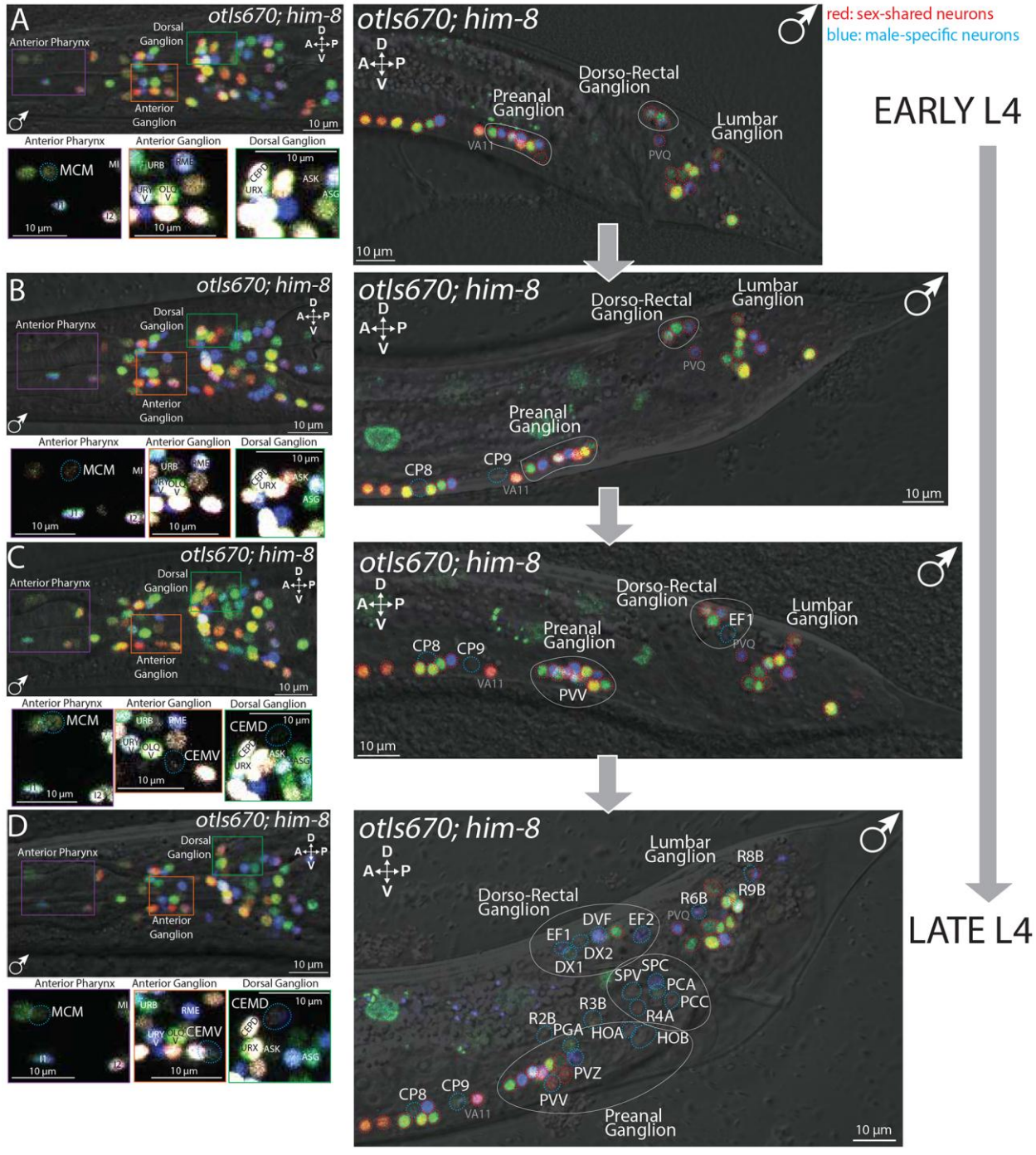

Fig.7: Just-in-time differentiation revealed by temporal appearance of NeuroPAL color codes.

Male-specific NeuroPAL (*otIs670; him-8*) neuronal color code emergence is coordinated with male maturation and retraction of the male tail, which occurs 4 hours before the L4-to-adult molt. The leftmost panel depicts representative images of NeuroPAL expression in the heads of L4 males. Inset images show NeuroPAL and the panneuronal marker in the following ganglia: the anterior pharynx (outlined in purple), anterior ganglion (outlined in orange), and dorsal ganglion (outlined in green). The right panel shows male-tail NeuroPAL expression and DIC from the early to late L4 larval stage. Sex-shared neurons are indicated with red dashed circles. Male-specific neurons are indicated with blue dashed circles and labeled with their neuron names. Some sex-shared neurons (*e.g.*, VA11 in the preanal ganglion and PVQ in the lumbar ganglion) are labeled to aid the reader in orienting themselves within the worm's ganglia. Each worm's head and tail were imaged in order to use the timing of the male-tail retraction to precisely define their age during the L4 larval stage – see Methods for further details on staging.

A: A representative image of an early L4 male NeuroPAL (*otIs670; him-8)* head with inset images from indicated regions below, and an age-matched male tail on the right. At this stage only sex-shared neurons and the male-specific neuron MCM express their NeuroPAL colors.

B: A representative image of a mid-early stage L4 male NeuroPAL (*otIs670; him-8)* head. Inset images from the indicated head regions are shown below and an age-matched tail on the right is shown that has just begun to retract. At this stage the male-specific neurons CP8 and CP9 are beginning to express their adult NeuroPAL color codes as indicated by the blue dashed circles.

C: A representative image of a mid-late stage L4 male NeuroPAL (*otIs670; him-8)* head. Inset images from the indicated head regions are shown below and an age-matched tail on the right is shown in which the tail tip hypodermal cells, hyp9 and hyp10, have retracted. At this stage in the head, the male-specific neurons CEMV and CEMD are beginning to express the panneuronal marker as indicated by the blue dashed circles. At this stage in the tail, the male-specific neurons PVV and EF1 are beginning to

express their adult NeuroPAL color codes as indicated by the blue dashed circles.

D: Representative image of a late stage L4 male NeuroPAL (*otIs670; him-8)* head. Inset images from the indicated head regions are shown below along with an age-matched tail. At this stage, many of the male-specific neurons are taking on their adult NeuroPAL color in the tail as indicated by the blue dashed circles.

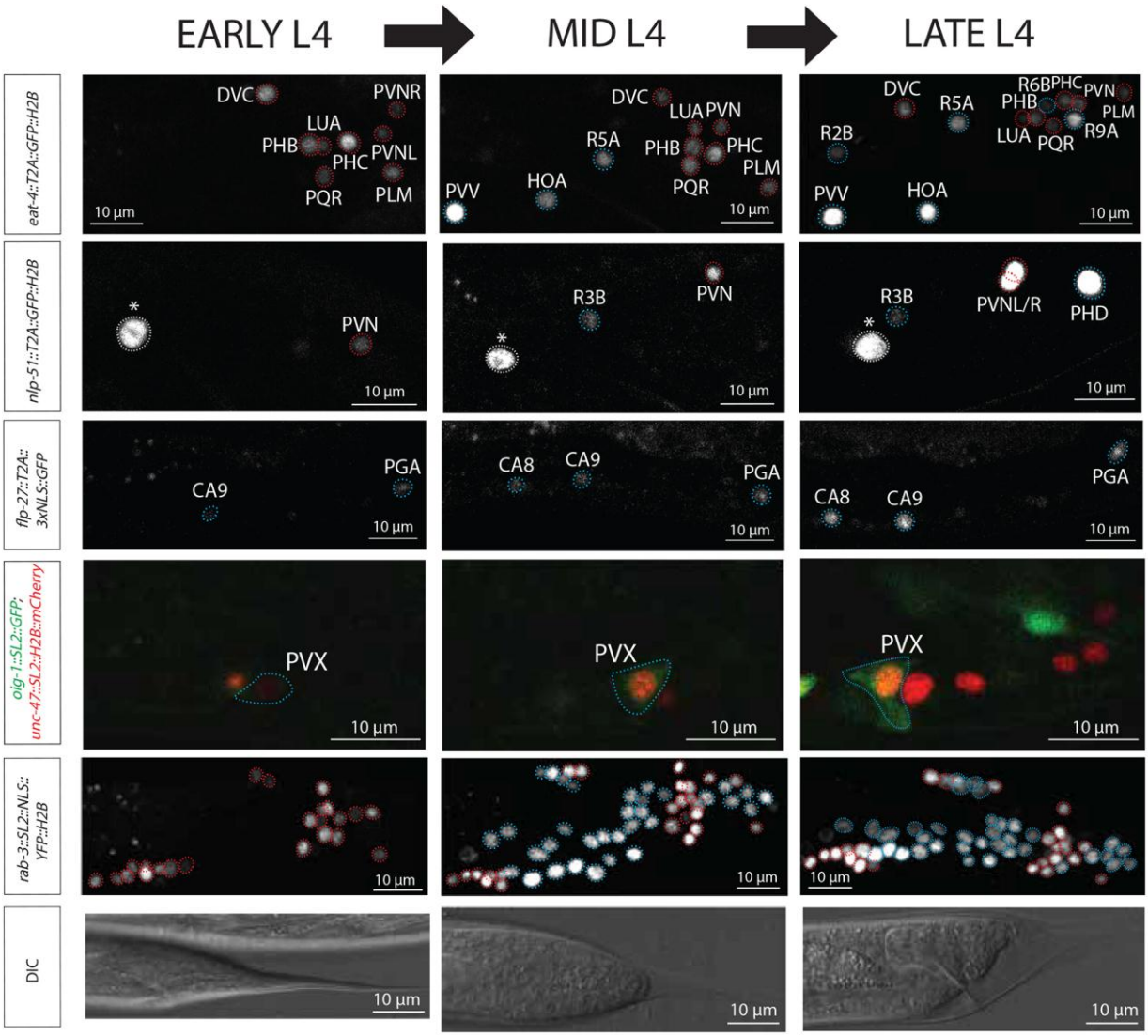

Fig.8: Just-in-time differentiation confirmed with additional reporter genes.

Expression of three fosmid-based reporters, the panneuronally expressed *rab-3* gene (*otIs498)*, the synaptic organizer *oig-1 (otIs450)*, and the vesicular transporter *unc-47 (otIs564)* as well as three reporter alleles in which endogenous genes were tagged with *gfp* through CRISPR/Cas9 genome engineering are shown, the neuropeptide encoding genes *flp-27(syb3213[T2A::3xNLS::GFP]), nlp-51(syb3936[SL2::GFP::H2B]),* and the vesicular glutamate transporter *eat-4(syb4257[T2A::GFP::H2B])*. Onset and/or strong upregulation was consistently observed during the mid-to-late L4 stage of development (see Methods for staging). Male-specific neurons are indicated with blue dashed circles

and, when possible, labeled with their neuron name. Sex-shared neurons are indicated with red dashed circles and, when possible, labeled with their neuron name. Non-neuronal cells are indicated with white dashed circles and an asterisk. In all cases except for *oig-1* and *unc-47,* NeuroPAL was used in the background to identify neurons.

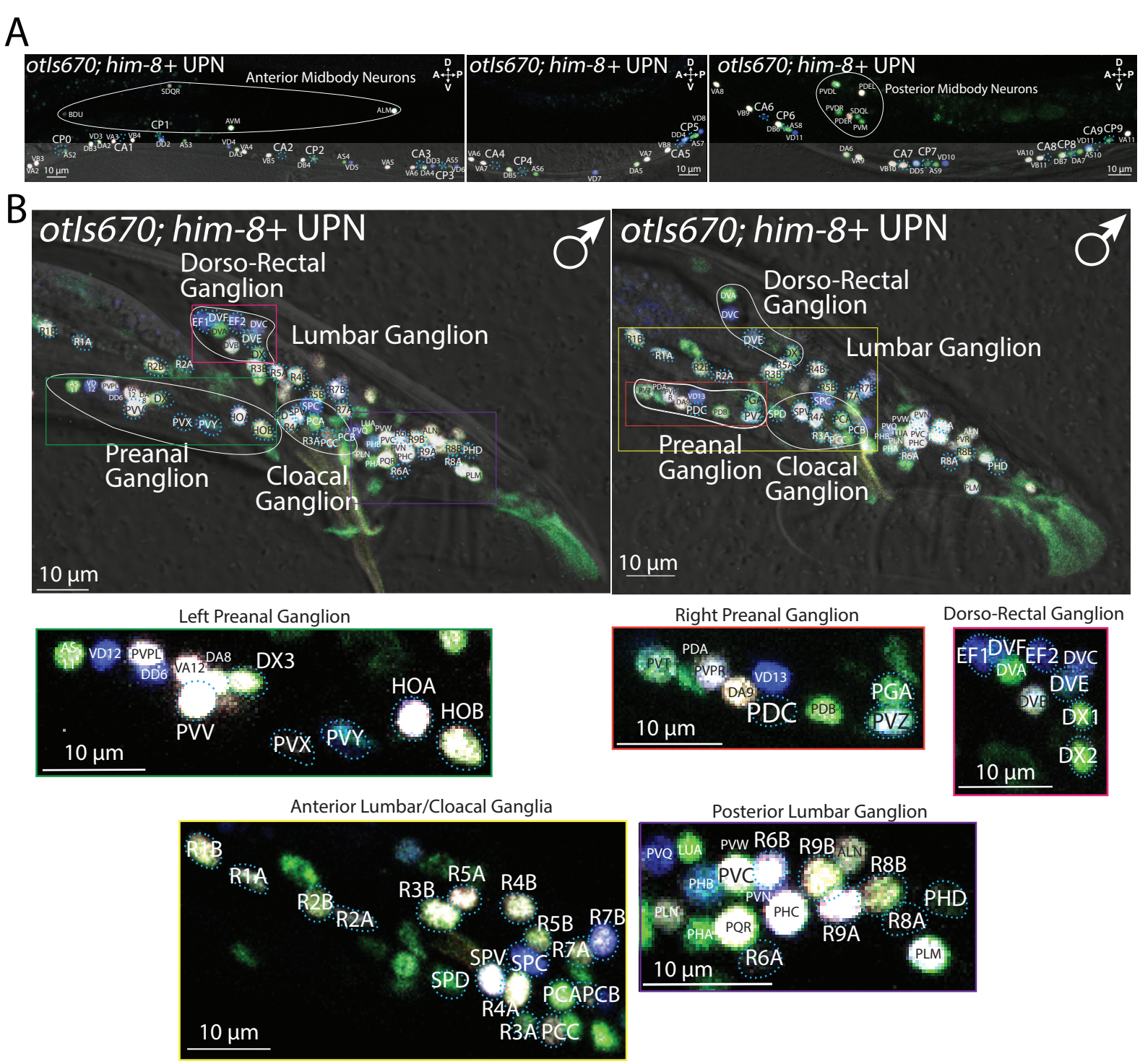

Fig. S1. Map of the adult, male-specific nervous system with panneuronal marker to visualize all neurons

A: Micrographs of stereotypic images from the midbody and ventral nerve cord (VNC) of adult male NeuroPAL (*otIs670; him-8)* worms from anterior to posterior. These images have the panneuronal (UPN) shown in white to visualize those neurons that express the panneuronal only (CA and CP neurons). All male-specific neurons are indicated with blue dashed circles.

B: Stereotypic micrographs of the left and right side of male NeuroPAL tails with zoomed in images of indicated regions below. These images have the panneuronal (UPN) shown in white to visualize those neurons that express the panneuronal only. These zoomed in images correspond to the left preanal ganglion (outlined in green), the right preanal ganglion (outlined in orange), the dorso-rectal ganglion (outlined in magenta), the anterior lumbar/cloacal ganglia (outlined in yellow), and the posterior lumbar ganglia (outlined in purple). All male-specific neuros are indicated with blue dashed circles. In response to our lasers, the male spicules exhibit yellow autofluorescence and the tip of the male fan exhibits green autofluorescence.

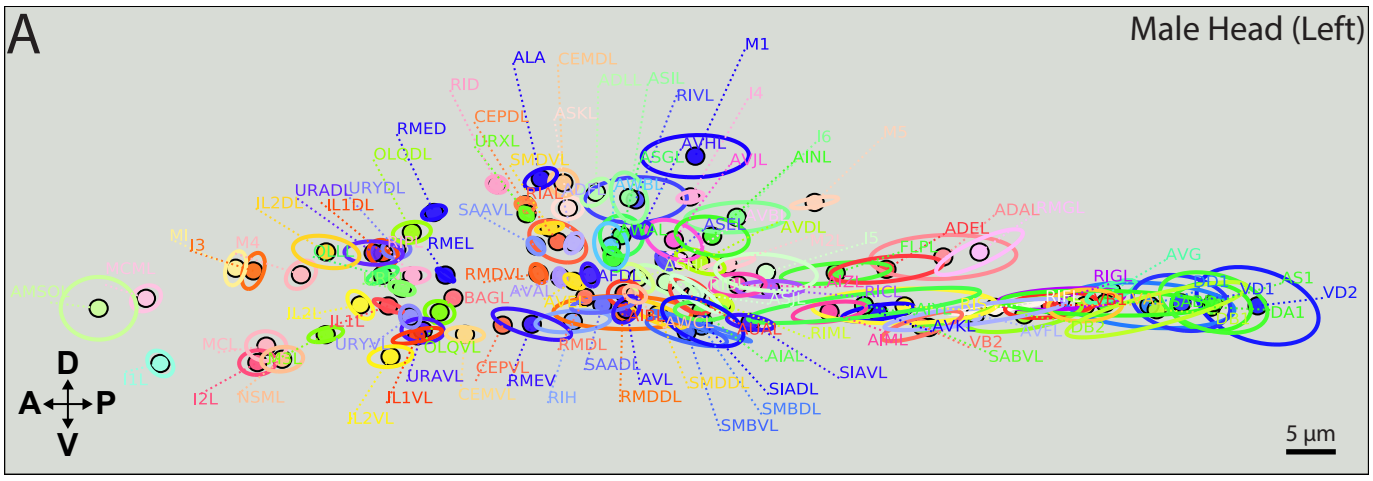

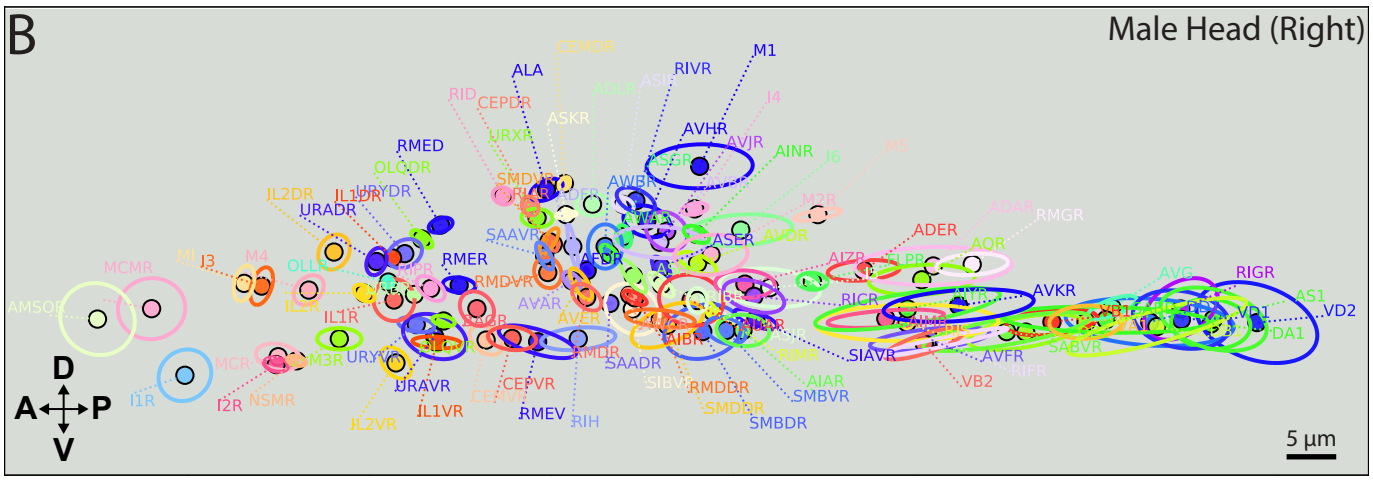

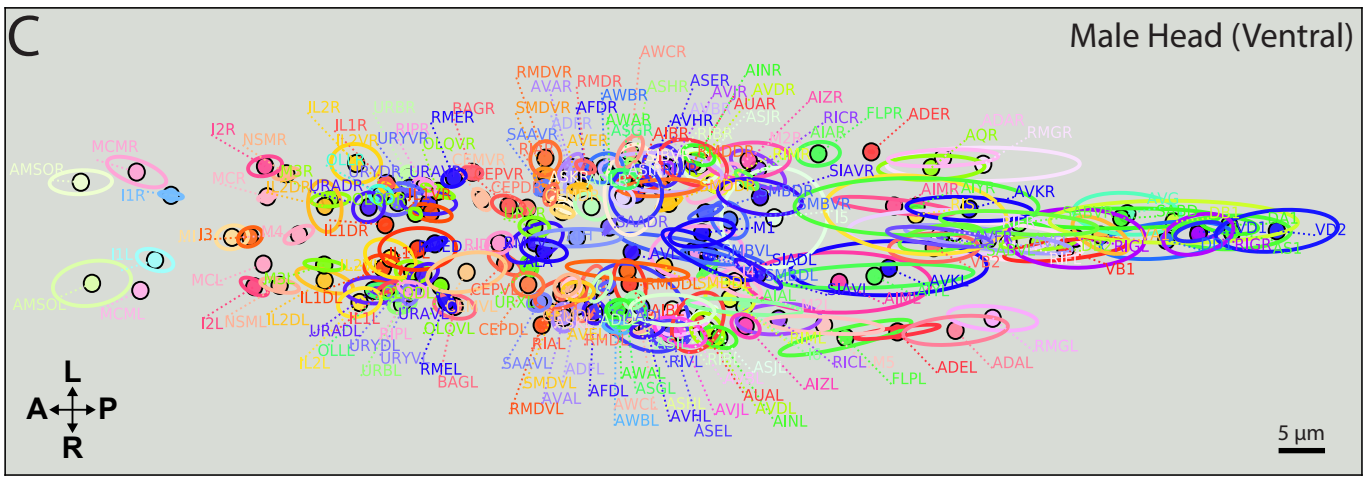

Fig. S2: Positional variability for male head neurons

A-C: The atlas of male head neuron positional variability (based on 12 male heads) for the left (A), right (B), and ventral (C) sided views. Dots indicate the mean position of each neuron. Ellipses indicate the positional variability of each neuron in the given axis. Neurons colors approximate those in NeuroPAL but have been brightened for visibility.

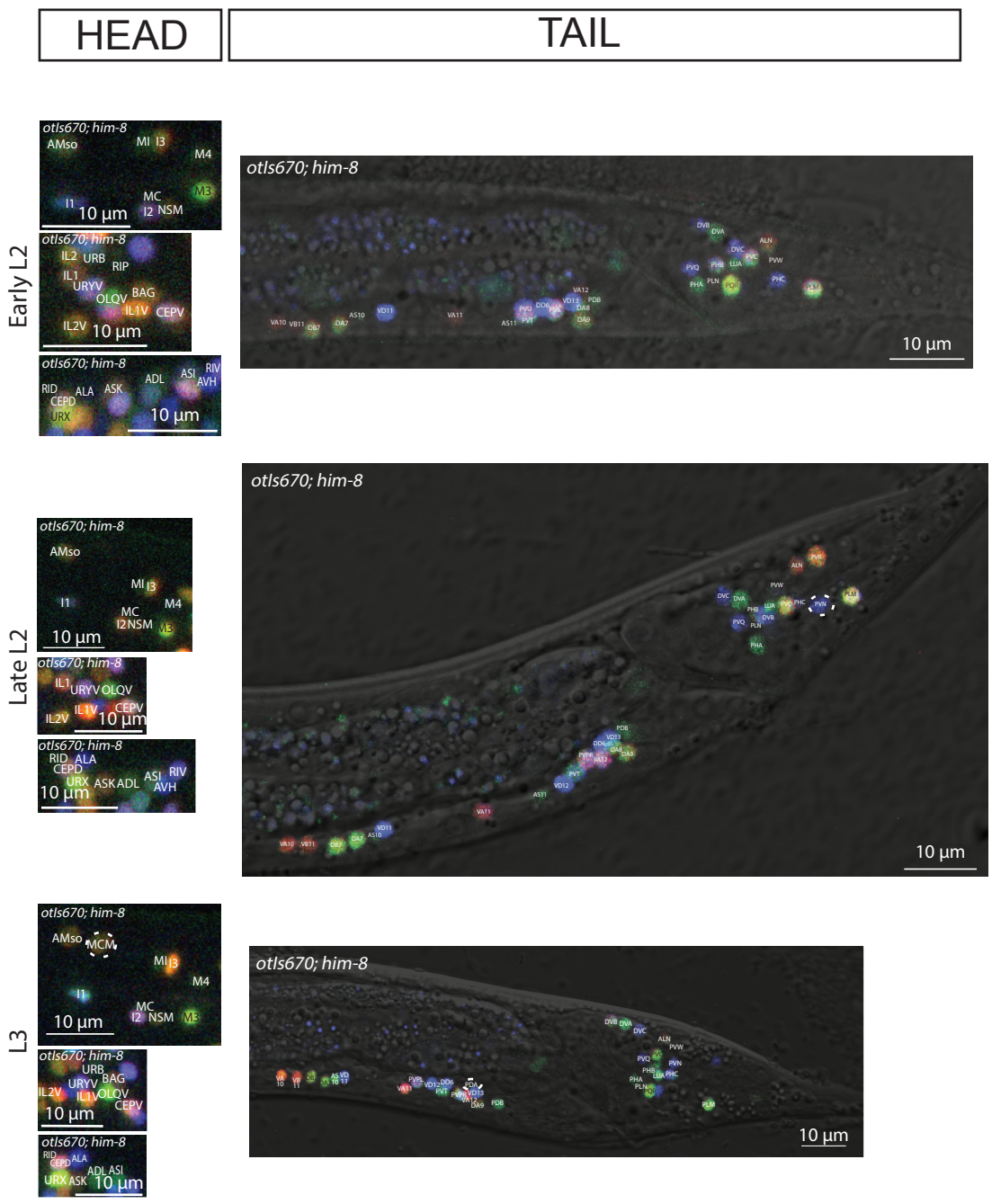

Fig. S3: L2 to L3 male NeuroPAL expression

Representative images of NeuroPAL expression (*otIs670;him*-8) in males. The larval stages shown are early L2, late L2, and L3.. The leftmost panel depicts representative images of NeuroPAL expression corresponding to the labeled larval stage. The regions shown (anterior to the pharynx, anterior ganglion, and dorsal ganglion) represent those where male-specific neurons are visible in the adult male head (the MCM and CEM neurons). The rightmost panel depicts representative images of NeuroPAL expression in male tails corresponding to the labeled larval stage.

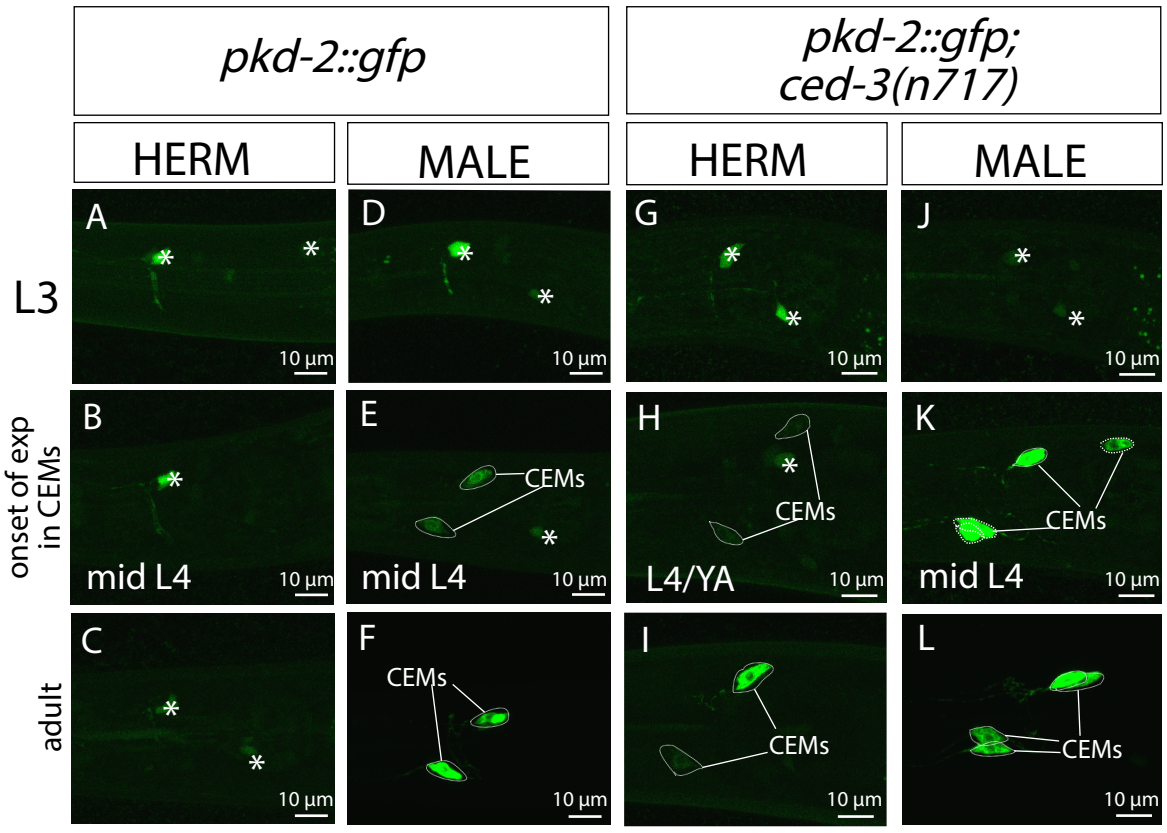

Fig. S4: Delayed gene expression in male-specific head neurons does not depend on sexual identity.

pkd-2::gfp (*myIs4*) expression in the male-specific CEM neurons is analyzed in a wild type (**A-F**) and a *ced-3(n717)* background (**G-L**). Images represent expression in L3 (**A,D,G,J**), adults (**C,F,I,L**), and the stage when *pkd-2::gfp* starts to become visible in the CEMs (**B,E,H,K**). YA: young adult. Asterisk: background expression, likely from the co-injection marker. In wild type, *pkd-2::gfp* expression comes on in males during the mid-L4 stage but never appears in hermaphrodites. In the *ced-3* cell-death mutant the CEM neurons do not die in hermaphrodites and *pkd-2::gfp* expression becomes visible within them during the L4/YA molt (panel H, L4/YA), then grows stronger in adults (panel I). Expression develops later in hermaphrodites than in males (panel K, mid L4), possibly due to a lower level of *pkd-2::gfp* expression in *ced-3* mutant hermaphrodites.

Table S1: List of all male-specific neurons and their NeuroPAL colors. Different promoters can drive the same reporter fluorophores. Thus the assignment of cell-specific color codes relies to a large extent on the examination of each reporter on its own. In the context of the male-specific nervous system, this has been done for some, but not all of these reporters. Wherever we have confirmed expression of the reporter in a neuron, its box is filled with the color corresponding to its reporter-fluorophore origin. Wherever we cannot be sure from where the color in a particular neuron originates, the box is filled with gray. Wherever we are sure a reporter is not expressed in a neuron, the box is left white.

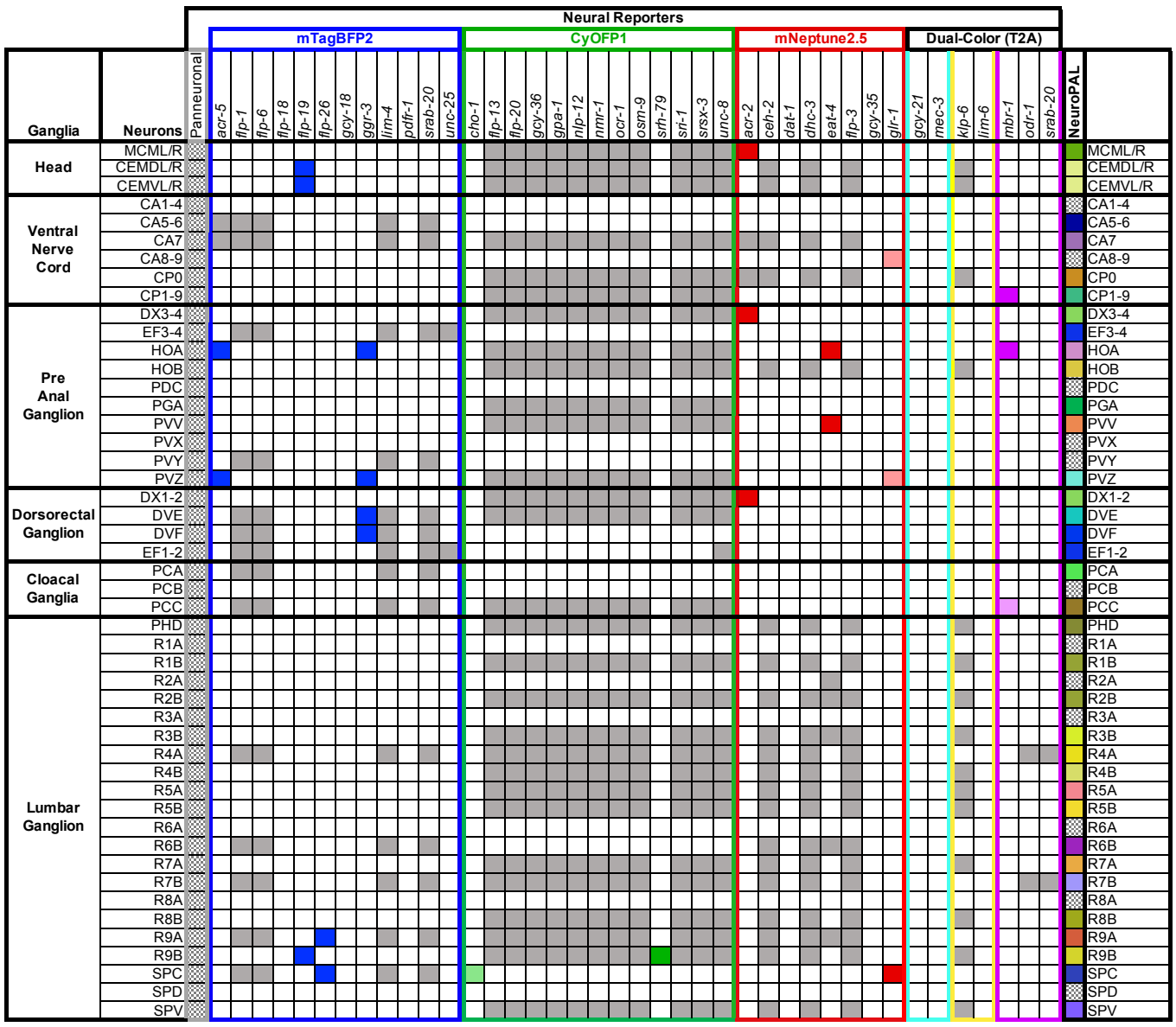

Colored boxes correspond to confirmed NeuroPAL expression.
Gray boxes coresond to NeuroPAL promoter fragments that may contribute to the neuron color code but were unable to be examined.
White boxes correspond to confirmed lack of expression of the promoter fragment in that neuron.

Table S2: Positional variability and color for all neurons in males and hermaphrodites

The positional and color variability of each neuron in the hermaphrodite and male head and tail. The results are based on 10 hermaphrodites, 12 male heads, and 13 male tails.

Table S2: Positional variability and color for all neurons in males and hermaphrodites

Neuron	mNeptune2.5	Variance	CyOFP1	Variance	mTagBFP2	Variance
ALNL	0.513979674	0.012659107	0.25942484	0.019572994	0.061233782	0.004092398
ALNR	0.402480365	0.012892629	0.223441998	0.004889851	0.093133701	0.003474661
AS10	0	0.014909718	1	0.03674995	0	0.004888448
AS11	0	0.018718505	1	0.039670358	0	0.00492238
CP9	0.013382622	0.01334303	0.603325569	0.045369383	0.045608132	0.011348598
DA7	0.427005284	0.069403708	0.909453076	0.03921332	0	0.009386299
DA8	0.625002388	0.046589391	0.796344423	0.028500388	0	0.01248373
DA9	1	0.062874914	0.328434367	0.050526571	0	0.011063524
DD6	0	0.009959324	0.145007734	0.015870271	1	0.056226665
DVA	0	0.012399259	1	0.027761294	0	0.006582076
DVB	0.323127483	0.017919609	0.193646864	0.011007097	0.367220197	0.030027543
DVC	0.100800914	0.010345333	0.076503886	0.010154277	0.630461369	0.04280557
DVE	0.259671665	0.034079131	0.409377674	0.018802915	0.323358257	0.018926018
DVF	0.148446298	0.004763642	0.072151389	0.006891429	0.484835605	0.032884963
DX1	0.084651571	0.006305561	0.681097745	0.051648072	0	0.009798846
DX2	0.046339378	0.012541174	0.77193577	0.042867645	0	0.006096295
DX3	0.122109284	0.009726202	0.866423055	0.047688714	0	0.007876951
EF1	0.048271794	0.00832086	0.020831434	0.009509495	0.676354045	0.088516357
EF2	0.096305691	0.004919426	0.051800761	0.00483717	0.567934221	0.041414015
EF3	0.052996958	0.048658595	0	0.008919325	0.864576755	0.088821544
HOA	0.769090136	0.105218176	0.067340352	0.00452127	0.383020487	0.028482753
HOB	0.384264012	0.007377327	0.362729859	0.011431483	0	0.002911015
LUAL	0	0.010218207	0.933934232	0.060977378	0	0.019688554
LUAR	0	0.012840643	1	0.053257425	0	0.010984492
PCAL	0	0.02028472	0.735232429	0.072346092	0	0.011425702
PCAR	0	0.015442767	0.957646357	0.060454345	0	0.015414591
PCBL	0.241733546	0.001237227	0.068072679	0.002118763	0.074180091	0.00159332
PCBR	0.256284736	0.001861724	0.092159602	0.004098859	0.071707731	0.001619011
PCCL	0.418746268	0.005915232	0.103304149	0.003043968	0.065618403	0.001034691
PCCR	0.431738562	0.019507304	0.101496261	0.002231978	0.061891297	0.001036656
PDA	0.260035471	0.004526873	0.135382954	0.007132997	0.068579627	0.011318283
PDB	0	0.043334861	0.954921874	0.096440763	0	0.020463909
PDC	0.19945918	0.011688189	0.174911417	0.047414224	0.060549171	0.0069585
PGA	0	0.008312043	0.582188358	0.049269793	0.079760154	0.012638634
PHAL	0	0.010386068	0.658487285	0.052457245	0.005987028	0.006194027
PHAR	0	0.006932243	0.668690312	0.020444599	0.018625129	0.003204963
PHBL	0.051962885	0.005699202	0.369985234	0.022590425	0.205441896	0.013152358
PHBR	0.034721955	0.002074337	0.390160362	0.015801796	0.251193582	0.019810718
PHCL	0.844942802	0.083117599	0.165955723	0.022083118	1	0.033241729
PHCR	0.749747784	0.106248574	0	0.007562155	1	0.082043544
PHDL	0.216513295	0.002954478	0.157814803	0.007015098	0.068592929	0.001878113
PHDR	0.213433194	0.002313543	0.125963471	0.002501662	0.082690384	0.000364194
PLML	0.447679211	0.08976585	1	0.042974507	0.091434986	0.025727321
PLMR	0.425486862	0.046140897	0.981894204	0.023083086	0.239586378	0.030043874
PLNL	0.342339441	0.003362895	0.260490731	0.007400891	0.105237529	0.002737626
PLNR	0.3582981	0.005297583	0.264323804	0.005557945	0.10548638	0.001056791
PQR	0.530902607	0.061820365	1	0.03758563	0	0.029495824
PVCL	0.390760983	0.032974131	0.940978048	0.066656135	0	0.038173438
PVCR	0.410908342	0.025349613	0.993846446	0.01818788	0	0.006831078
PVNL	0.160065936	0.004506464	0	0.009231331	0.771444308	0.09086092
PVNR	0.270565514	0.045489079	0	0.012965889	0.956194443	0.071421241
PVQL	0.76937888	0.037517682	0.197703683	0.013118668	0.838723634	0.066982209
PVQR	0.616827414	0.039295658	0.15467876	0.008719371	0.694821931	0.112157425
PVR	0.097792312	0.004991148	0.067763896	0.002286884	0.48639185	0.022792946
PVS	0.084494336	0.003134998	0.047407422	0.001300954	0.596311721	0.027604194
PVT	0.661635906	0.02784985	0.582084022	0.030102739	0	0.004056396
PVU	0.134457722	0.015084219	0.654703749	0.021319069	0.109731014	0.004111976
PVV	1	0.044001474	0	0.014541881	0.278082397	0.009496603
PVWL	0.25624455	0.002235276	0.087951184	0.001424871	0.096334629	0.001876105
PVWR	0.258220659	0.003644709	0.112075252	0.003079141	0.084382979	0.000511479
PVX	0.231750432	0.001028014	0.068484	0.001469618	0.093130521	0.000680811
PVY	0.215343142	0.002124674	0.065823511	0.002569541	0.170859578	0.00169453
PVZ	0.137129726	0.017262203	0.483995837	0.038946366	0.268573379	0.041260049
R1AL	0.245686277	0.002099005	0.065963026	0.002794563	0.085453486	0.000690061
R1AR	0.233495991	0.000496552	0.093524183	0.002314733	0.080023826	0.001000741
R1BL	0.471658346	0.019352028	0.294263584	0.018245596	0.018852154	0.005866994
R1BR	0.451277689	0.012539234	0.302222302	0.013365194	0.014169478	0.004075544
R2AL	0.205701257	0.005614642	0.104267786	0.012888987	0.08413267	0.001372577
R2AR	0.223627702	0.001078941	0.086543826	0.002057392	0.107948658	0.002036668
R2BL	0.307572884	0.004279104	0.221629899	0.007242615	0.053699348	0.002340653
R2BR	0.375190146	0.007142206	0.28077818	0.006449095	0.024427882	0.001736717
R3AL	0.212396646	0.000988979	0.164283741	0.00443397	0.058509019	0.001356574
R3AR	0.216711978	0.001909788	0.150879128	0.002528526	0.079210044	0.000912905
R3BL	0.475911251	0.016731378	0.37963562	0.015331701	0.040086844	0.002794831
R3BR	0.536665177	0.018200664	0.492380926	0.023976812	0	0.005623798
R4AL	0.724956963	0.046766588	0.371403131	0.02829487	0	0.005120361
R4AR	0.676837495	0.027499933	0.478567579	0.028779524	0	0.012267661
R4BL	0.471276181	0.015788391	0.337696086	0.032164686	0.045492008	0.005483918
R4BR	0.546973445	0.037402289	0.320784964	0.018293416	0.093569146	0.004636524
R5AL	1	0.110080733	0	0.008487854	0.193897852	0.005557801
R5AR	0.955414685	0.131572263	0.028931634	0.005491409	0.194217608	0.001520628
R5BL	0.389620727	0.00690812	0.277030241	0.007399315	0.038949036	0.002292371
R5BR	0.406527058	0.014126103	0.351550353	0.009096357	0.009484719	0.003224
R6AL	0.215430064	0.00593093	0.180108431	0.007639613	0.07952198	0.001464814
R6AR	0.202449461	0.008988475	0.120461203	0.014002885	0.12186113	0.002328152
R6BL	0.258370469	0.001044384	0.021654294	0.005674936	0.442339549	0.079426017
R6BR	0.343201426	0.012620657	0.053191648	0.003823936	0.449945885	0.073000059
R7AL	0.362887513	0.004109935	0.175936076	0.0051645	0.098578702	0.005532962
R7AR	0.308517503	0.003857318	0.170874376	0.005672127	0.128362466	0.02207733
R7BL	0.226957669	0.009251001	0.087561213	0.006800757	0.768218979	0.110594499
R7BR	0.215009836	0.010580215	0.0952559	0.004740099	0.829433212	0.092998339
R8AL	0.306005865	0.011138011	0.208847185	0.009914301	0.046419239	0.001047089
R8AR	0.288465333	0.010033817	0.118702161	0.002120261	0.070463319	0.000658256
R8BL	0.452124118	0.005100238	0.349187968	0.018044723	0.00114193	0.005399357
R8BR	0.465691284	0.013174863	0.300561557	0.00626833	0.018939379	0.003577594
R9AL	1	0.158333628	0	0.013390904	0.344773972	0.003230748
R9AR	0.905812645	0.144066375	0	0.006010347	0.511390862	0.083720552
R9BL	0.515410152	0.008831055	0.395663292	0.020663765	0	0.005718967
R9BR	0.696148909	0.050442936	0.407784502	0.025767833	0	0.00595756
SPCL	0.05030194	0.011060704	0.020997085	0.007145273	0.691862315	0.106697485
SPCR	0.004886725	0.009856685	0	0.006439039	0.833998111	0.084961046
SPDL	0.180127535	0.002516355	0.220962499	0.007187675	0.06947952	0.00187491
SPDR	0.186247301	0.005247328	0.263165809	0.014750851	0.049477711	0.004048986
SPVL	0.410097915	0.016226977	0.324448966	0.01110893	0.191786729	0.017225806
SPVR	0.346237223	0.023663935	0.371994735	0.013821724	0.383709733	0.026587473
VA11	1	0.184029365	0	0.00938491	0.595035929	0.033250324
VA12	1	0.101004645	0	0.006001055	0.42396224	0.019535848
VD11	0	0.007239745	0	0.008041301	1	0.102077211
VD12	0	0.006156207	0	0.010005264	1	0.119060575
VD13	0	0.008786427	0	0.009146446	1	0.082197311